

Atomic Absorption Line Diagnostics for the Physical Properties of Red Supergiants

BROOKE DICENZO¹ AND EMILY M. LEVESQUE²

¹*University of Washington, Seattle, WA 98195*

²*Department of Astronomy, University of Washington, Seattle, WA 98195, USA*

ABSTRACT

Red supergiants (RSGs) are evolved massive stars that represent extremes, in both their physical sizes and their cool temperatures, of the massive star population. Effective temperature (T_{eff}) is the most critical physical property needed to place a RSG on the Hertzsprung-Russell Diagram, due to the stars' cool temperatures and resulting large bolometric corrections. Several recent papers have examined the potential utility of atomic line equivalent widths in cool supergiant spectra for determining T_{eff} and other physical properties (Dorda et al. 2016a,b) and found strong correlations between Ti I and Fe I spectral features and T_{eff} in earlier-type cool supergiants (G and early K) but poor correlations in M-type stars, a spectral subtype that makes up a significant fraction of RSGs. We have extended this work by measuring the equivalent widths of Ti, Fe, and Ca lines in late K- and M-type RSGs in the Milky Way, Large Magellanic Cloud, and Small Magellanic Cloud, and compared these results to the predictions of the MARCS stellar atmosphere models. Our analyses show a poor correlation between T_{eff} and the Fe I and Ti I lines in our observations (at odds with strong correlations predicted by stellar atmosphere models), but do find statistically significant correlations between T_{eff} and the Ca II triplet (CaT) features of Milky Way RSGs, suggesting that this could be a potential diagnostic tool for determining T_{eff} in M type supergiants. We also examine correlations between these spectral features and other physical properties of RSGs (including metallicity, surface gravity, and bolometric magnitude), and consider the underlying physics driving the evolution of atomic line spectra in RSGs.

1. INTRODUCTION

Red supergiants (RSGs) represent a critical phase in massive stellar evolution. They are He-fusing evolved descendants of 10-25 M_{\odot} main sequence stars, the end result of a nearly horizontal evolution across the Hertzsprung-Russell (H-R) diagram as their blue H-fusing predecessors leave the main sequence and cross the “yellow void”. They are the largest (in physical size) and coldest (~ 3500 -4500 K) members of the massive star population, representing a significant extreme in their evolution. These cool temperatures place them at the Hayashi limit for hydrostatic equilibrium (Hayashi & Hoshi 1961).

Effective temperature (T_{eff}) is, along with bolometric luminosity (M_{bol}), one of the two key physical properties needed to place a star on the Hertzsprung-Russell (H-R) diagram, and it is the most critical physical property that must be determined for RSGs. At these cool

temperatures, the bolometric corrections for standard *UBVRI* photometry are large (1-4 mag) and strongly dependent on T_{eff} (e.g. Massey & Olsen 2003; Levesque et al. 2005); as a result, accurately calculating the luminosity of a RSG requires a robust determination of the star's T_{eff} .

The scarcity of nearby RSGs has limited the use of interferometric data in ascertaining an accurate T_{eff} scale (see, for example, Dyck et al. 1996). Alternatively, scales in the past have been determined by broad-band colors of RSGs with known diameters (Lee 1970; Johnson 1964, 1966) or by bolometric corrections derived from IR measurements under the assumption of a blackbody continuum (Flower 1975, 1977). However these methods are also limited because of the effects of line blanketing, which make color indices such as $B - V$ highly sensitive to surface gravity ($\log g$). More recently, Levesque et al. (2005, 2006) used the MARCS stellar atmosphere models to fit the strengths of the T_{eff} -sensitive TiO bands for K-type and M-type stars in the Milky Way and Magellanic Clouds, creating a T_{eff} scale significantly warmer than previous works (Humphreys & McElroy 1984; Massey & Olsen 2003) and one that

dicenzob@uw.edu

emsque@uw.edu

shows good agreement with the predictions of stellar evolutionary tracks (including the metallicity dependence of the Hayashi limit). Davies et al. (2013) determined warmer T_{eff} values for RSGs using broad SED fitting across the optical and near-IR. However, these results do not reproduce the correlation between spectral type and T_{eff} in RSGs or the metallicity dependence of RSG T_{eff} s (see, for example, Levesque et al. 2006; Tabernero et al. 2018), and the work notes that 3D models (as opposed to the 1D MARCS models) are required to properly account for wavelength-dependent in the extended atmospheres of RSGs that would otherwise lead to determining a warmer T_{eff} at longer wavelengths.

Several recent papers have also examined the potential utility of atomic lines in these cool stars' spectra for determining T_{eff} and other physical properties. Dorda et al. (2016a) compared the widths of several atomic lines (including Fe I and Ti I features and the Ca II triplet lines at 8498Å, 8542Å, and 8662Å, hereafter CaT) observed in the spectra of a large sample of cool supergiants (CSGs, ranging from G0 to M7 in spectral type and thus encompassing the late-type yellow supergiant population as well as RSGs) in the Large and Small Magellanic Clouds; they found that the strength of the Ti I lines was strongly correlated with T_{eff} (though no similar correlation was seen for Fe I or CaT). This result was further supported by Dorda et al. (2016b), which successfully used a principal component analysis based on spectral features in the CaT region (the same region covered by the Gaia Radial Velocity Spectrograph) to automatically differentiate CSGs from other bright late-type stars. This is potentially a very exciting result, offering the possibility of determining T_{eff} for RSGs from data with relatively limited wavelength coverage (as opposed to existing methods which require optical+IR photometry or spectrophotometry with wide optical wavelength coverage). Tabernero et al. (2018) studied the T_{eff} scale of CSGs in different metallicity environments; while their method adopted atomic line fitting as a means of determining T_{eff} they found a warmer and shallower scale than Levesque et al. (2006), with only a weak correlation in the LMC and no correlation in the SMC.

However, the utility of using atomic line features for determining T_{eff} in RSGs is still unclear. While the correlation between Ti I and spectral type presented in Dorda et al. (2016a) is quite robust at earlier types (G and early K), the correlation is much weaker for the M-type stars in their sample, which represent a significant fraction of the RSG population. The potential dependence of these features on other physical properties is also a complicating factor. For example, recent obser-

vations of RSG J -band spectra in nearby galaxies have revealed that, while atomic absorption features such as Ti I, Fe I, and Si I are not strongly sensitive to T_{eff} , they serve as excellent probes of metallicity (e.g. Davies et al. 2010, 2015; Gazak et al. 2015; Patrick et al. 2015, 2016, 2017).

The CaT is widely cited as a potential tracer of luminosity class in cool stars due to its sensitivity to $\log g$ effects (e.g. Cenarro et al. 2001a,b and references therein), and is also sensitive to metallicity (e.g. Armandroff & Da Costa 1991; Sakari & Wallerstein 2016). Non-LTE effects in the atmospheres of these stars can also impact the equivalent widths (EWs) of some lines; Jennings & Levesque (2016) found that the H α absorption feature in cool stars is also effective as a luminosity class diagnostic, a consequence of the density-dependent overpopulation of the metastable 2s level and an effect that becomes stronger in the non-LTE conditions present in supergiant atmospheres. The Jennings & Levesque (2016) study of the CaT feature indicated that while the feature in early M-type stars had a clear relationship with luminosity class, as supported by the literature, this relationship also broke down in late-type (beyond M3-3.5) supergiants.

Previous work on the CaT has studied its effectiveness as a diagnostic for several physical parameters such as luminosity, $\log g$, metallicity, and T_{eff} . The CaT is a near-IR feature and therefore is subject to contamination from multiple strong stellar features such as higher-order Paschen lines and the TiO absorption band at 8433Å. Ginestat et al. (2016) studied the relationship between the EW of absorption features between 8380–8780 Å and spectral type, finding a positive correlation between CaT and luminosity for A to M type stars that was initially weak but began to increase for later types beginning at G0. Ginestat also proposed that the weak Ca I, Ti I, and Fe I lines of the *giants* in their study may be due to low metallicity.

Erdelyi-Mendes & Barbuy (1990), hereafter EM&B, used synthetic stellar atmosphere models from Gustafsson et al. (1975) to generate synthetic CaT lines in order to examine their variation with T_{eff} , $\log g$, and metallicity ($[M/H]$). EM&B found the CaT to be primarily dependent on $[M/H]$ and $\log g$. Their study indicates that the CaT is sensitive to metallicity for stars with $[M/H] > -2.0$ and sensitive to $\log g$ for giants with $[M/H] > -1.0$. EM&B also found that the relationship between CaT and temperature is only present in low $\log g$ populations, making it applicable to giants and supergiants rather than dwarf stars, and becomes more pronounced as metallicity increases. This is in agreement with the results of Smith & Drake (1990) but it should be noted

that their work was restricted to stars between 4000 and 5500 K. When compared against T_{eff} , EM&B found only a weak relationship between the CaT triplet and T_{eff} , which they attributed to the increasing intensity of the 8433Å TiO feature at cool temperatures. The increasing strength of this TiO band can lead to a decrease in the local continuum and a subsequent apparent weakening of the CaT (as noted by [Ginestet et al. 2016](#), who used a local continuum definition for measuring the CaT in stars later than M2 in order to account for this effect); however, this particular TiO band is only prominent in the spectra of RSGs with relatively late spectral types (\sim M4-M5, e.g. [Levesque et al. 2005](#); [Massey et al. 2017](#)), an effect in agreement with the evolution of the CaT seen in [Jennings & Levesque \(2016\)](#).

[Mallik \(1996\)](#) analyzed the CaT features of 146 stars spanning from F7 to M4 to determine the dependence of CaT on luminosity, T_{eff} , and metallicity. They found a non-linear relationship for luminosity that became more pronounced with increased metallicity, and that was more apparent in supergiants than in dwarfs, but did not find a relationship between CaT and T_{eff} across the full sample. Mallik also found that at low $\log g$ (0.0 to 2.0), the EW of the CaT in supergiants and giants decreased as $\log g$ increased. This correlation - which is counter to the typical expectation that lines will get stronger at higher $\log g$ due to increased collisional effects - has been explained as a continuum effect. An increase in the continuous absorption coefficient at higher $\log g$ (due to an increased electron density in stars where H^- is the dominant source of continuum opacity) leads to a lower apparent continuum level and subsequent weaker measurements of EW for the CaT.

[Cenarro et al. \(2001a\)](#) presented a new stellar library of the near-IR spectral region based on 706 stars with $2750 \text{ K} < T_{\text{eff}} < 38400 \text{ K}$, $0.0 < \log g < 5.12$, and metallicities of $-3.45 < [\text{Fe}/\text{H}] < +0.60$. Based on these data they offer a newly defined index for measuring the strength of the CaT features, the ‘‘CaT*’’ index, developed with careful treatments of previously noted effects such as continuum definition and Paschen line contamination.

Collectively, the utility of the CaT feature has been extensively studied, but conclusions about its use as a diagnostic of $\log g$, luminosity, and T_{eff} are conflicting and further complicated by the differing sample sizes and parameter spaces of previous works, with most samples of stars spanning from dwarfs to supergiants and covering a broad range of spectral types. In this work we specifically consider the utility of atomic absorption line features as potential T_{eff} diagnostics in the uniquely cool and low-density environments of M-type RSGs.

We present a study examining the strengths of Ca, Ti, and Fe absorption features in the spectra of M-type RSGs. Using echelle spectra of 25 Milky Way RSGs, 16 Large Magellanic Cloud RSGs, and 17 Small Magellanic Cloud RSGs along with a series of RSG model atmosphere spectra (Section 2), we present the EWs of a large sample of atomic lines, including features of Fe I, Ti I, Ca I, and the CaT, and compare these EWs to the T_{eff} determinations of [Levesque et al. \(2005; Section 3\)](#). We find a strong positive and statistically significant correlation between CaT and T_{eff} for Milky Way RSGs, but no similar correlation in the Magellanic Cloud samples, and no relationship between the Ti I and Fe I features and T_{eff} as a function of metallicity (Section 4). We discuss the implications of these results for understanding the physical properties of RSGs as well as potential future work in this area (Section 5).

2. SAMPLES AND OBSERVATIONS

The RSG echelle spectra used in these analyses were originally observed as part of a spectroscopic search for potential Thorne-Żytkow objects in the Milky Way and Magellanic Clouds ([Levesque et al. 2014](#)). The sample of 25 Milky Way stars was selected from the coldest RSGs identified in [Levesque et al. \(2005\)](#); all have spectral types of K5-M0I or later. The spectra were observed using the Astrophysics Research Consortium Echelle Spectrograph (ARCES; [Wang et al. 2003](#)) on the Apache Point Observatory 3.5-m telescope on 2011 February 11 and 12 (UT). The observations were taken using the default $1.6 \text{ arcsec} \times 3.2 \text{ arcsec}$ slit, along with quartz lamps and ThAr lamps after each individual exposure to achieve precise flat-field and wavelength calibrations for each star. The spectra were reduced using standard IRAF¹ echelle routines, and each star’s spectrum was corrected for radial velocity (RV) effects using the wavelengths of the CaT triplet. Examples of our spectra and the CaT triplet are shown in Figure 1.

Our Magellanic Cloud sample was drawn from late-type RSGs identified in [Levesque et al. \(2006\)](#) and supplemented by additional stars with broadband colors consistent with RSGs (for a complete discussion see [Levesque et al. 2014](#)). These stars were observed with the Magellan Inamori Kyocera Echelle (MIKE; [Bernstein et al. 2003](#)) on the Magellan 6.5-m at Las Campanas Observatory during 2011 September 13-15. The spectra were taken using the $0.7 \text{ arcsec} \times 5 \text{ arcsec}$ slit with 22 binning, slow readout, and the standard grating settings, and internal flats and ThAr lamps were ob-

¹ IRAF is distributed by NOAO, which is operated by AURA, Inc., under cooperative agreement with the NSF.

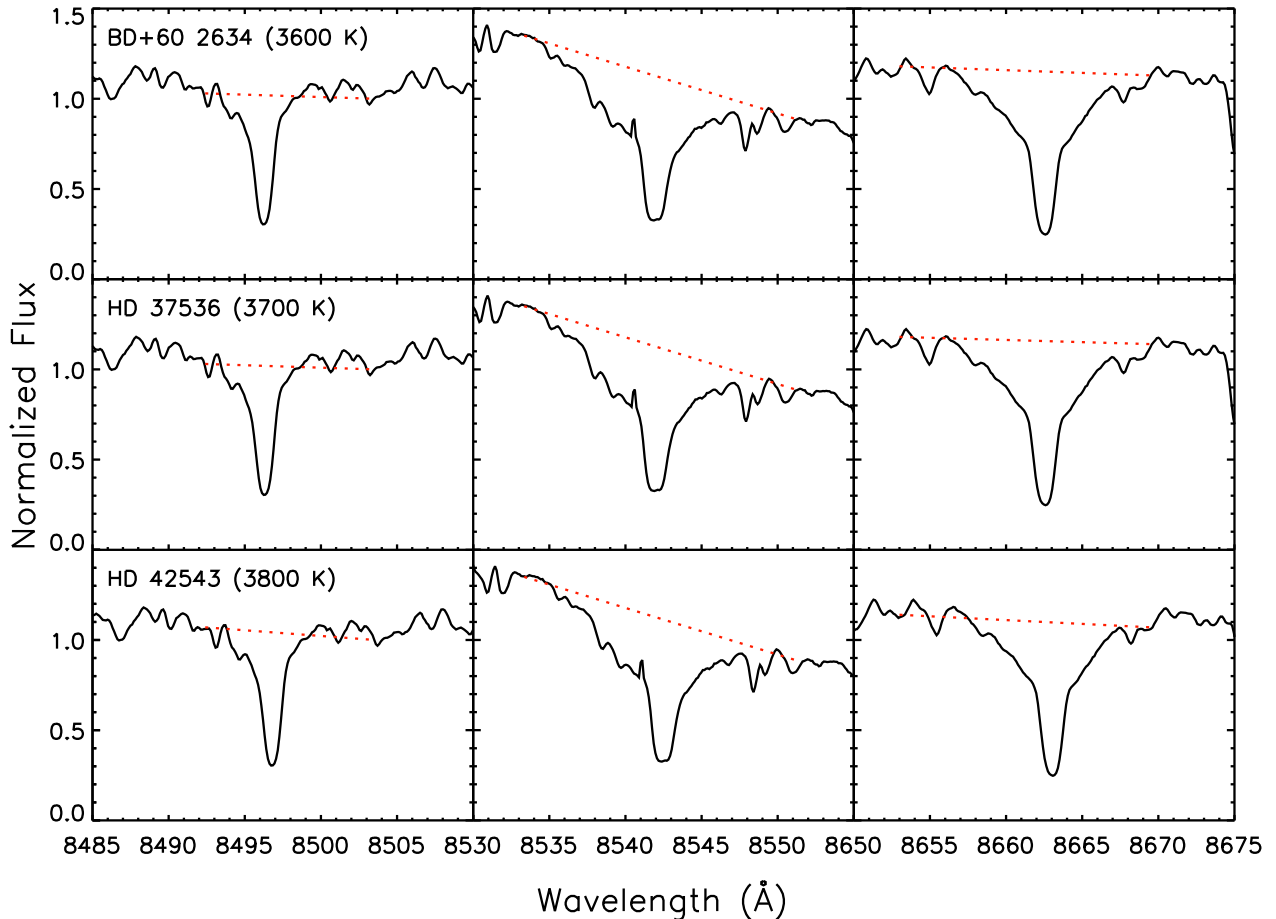


Figure 1. Example normalized spectra of the Ca II 8498Å (left), 8542Å (center), and 8662Å (right) absorption triplet features for three Milky Way RSGs in our sample, spanning a 200 K range in T_{eff} . The spectra are shown in black, while the “pseudocontinua” - defined by the continuum points listed in Table 2 and described in §3.1 - used for fitting the lines and determining their equivalent widths are illustrated as dashed red lines.

served for flat-fielding and wavelength calibration purposes. These data were reduced using a combination of standard IRAF echelle routines and the `mtools` package. The Thorne-Zytkow object candidate HV2112 is not included in our sample.

The physical properties of the observed stars in our sample that we adopt for our analyses - including T_{eff} , $\log g$, and M_{bol} - are drawn from Levesque et al. (2005, 2006), and are based on fitting observed spectrophotometry of the RSGs with MARCS stellar atmosphere models and determining the best-fit model based on the strengths of the TiO absorption bands and the overall fit of the SED. This T_{eff} scale was chosen as it represents physical properties for RSGs determined based on the optical regime and optical absorption features, an appropriate choice for comparison with the optical atomic line features used in this work as it samples the same physical region of the RSG atmosphere (recalling these stars’

extended geometries and wavelength-dependent optical depths, as discussed above). These T_{eff} scales also show good agreement with stellar evolutionary models (including those that treat both single and binary evolution; Levesque 2018 and the effects of metallicity. For a complete list of the stars in our sample and their adopted physical properties, see Table 1.

Tabernero et al. (2018) recently published a new T_{eff} scale for CSGs in the LMC and SMC; however, this scale is based on atomic line fitting and the assumption we wish to test here, namely that these lines T_{eff} -sensitive. For late K- and M-type RSGs the Tabernero et al. (2018) scale is slightly warmer than the Levesque et al. (2006) scales as well as shallower (a weaker dependence on spectral type), but without knowing the dependence of the individual atomic features on T_{eff} in this very cool regime it is unclear whether this disagree-

ment is due to a difference in method or a consequence of the lines' behavior (for further discussion see §4.)

In addition to our sample of observed RSG spectra we also consider synthetic spectra produced by the MARCS stellar atmosphere models (e.g. Gustafsson et al. 2008). The spectra were generated for solar-metallicity $15M_{\odot}$ RSGs and adopt a spherical atmosphere geometry, a microturbulence parameter of 5 km s^{-1} , and $\log g = -0.5, 0.0, 0.5, 1.0$. The T_{eff} of the models used in this work range from 3400-4000K in 100K increments.

It should be noted that we restrict our use of the MARCS models to $T_{\text{eff}} \leq 4000 \text{ K}$, and do the same for our observed sample (one LMC star from the original Levesque et al. 2014 sample, LMC 169754, was cut from this work due to its relatively high T_{eff} of 4100 K). This was done specifically to restrict our study of atomic line T_{eff} diagnostics to the collision-dominated regime of cool star atmospheres (at $T_{\text{eff}} \gtrsim 4000\text{K}$ the effects of photoionization increasingly dominate the abundance of neutral Fe and Ti) and a regime where non-LTE effects are minimal; for further discussion see Section 4.

3. ANALYSES

3.1. Atomic Lines and Equivalent Widths

We measured the EWs of absorption line features of Fe I, Ti I, Ca I, and Ca II in each of our spectra, using the line profile fitting function contained in the `splot` task in IRAF's `kpnsplit` package to determine the best-fit Voigt profile. The Ca features include Ca I 6572Å and the CaT, while the Fe I and Ti I absorption features measured are the same as those used in Dorda et al. (2016a). Upper and lower wavelength bounds were set by identifying the closest local maxima in the surrounding region of the spectrum to define a local continuum which could then be used to measure integrated line strengths; where possible the upper and lower bounds were selected to match the analyses of (Dorda et al. 2016a; see Table 2). These local continua were defined consistently across all of the stars in a given host galaxy, although slight variations in the local continuum definition were necessary between the three host galaxies in the case of the CaT lines.

The full set of absorption lines and their measured EWs are given in tables 3-5 for Ca, Fe, and Ti features respectively, and in Table 6 for the MARCS models.

3.2. Correlation Coefficients

We used the `matplotlib` `PyLab` software from `SciPy` to plot the measured EW data against the T_{eff} , M_{bol} , and $\log g$ of each star as determined by Levesque et al. (2005, 2006), with EW as the dependent variable and the stel-

lar parameters as the independent variable. For each variable pair we also calculated the Pearson's r correlation coefficient and associated p -value for the sample, along with both linear ($Ax+B$) and second-degree polynomial (Ax^2+Bx+C) functions of best fit. Given our small sample sizes (ranging from 16 to 25 stars in a given host galaxy, which we treat separately due to metallicity effects) we adopt a conservative significance threshold of $p < 0.01$, rather than the more typical $p < 0.05$, to decrease our likelihood of incorrectly rejecting the null hypothesis. The Pearson correlation coefficients and best-fit function coefficients are summarized in Table 7. A similar analysis was also done for the MARCS stellar atmosphere model spectra, with the results summarized in Table 8.

Below we consider each spectral feature and its potential diagnostic utility:

CaT: In our Milky Way sample, the equivalent width of the CaT feature (Figure 2) shows a strong and statistically significant positive correlation with T_{eff} , with Pearson's $r=0.755$ and $p=0.00001$. This is in good agreement with the MARCS stellar atmosphere models at Milky Way metallicity (Figure 8), which predict robust positive correlations between CaT and T_{eff} across the full range of supergiant surface gravities (e.g., Pearson's $r=0.869$ and $p=0.0023$ for the $\log g = 0.0$ models). However, no similar correlation is seen in the LMC and SMC samples, despite the LMC- and SMC-metallicity MARCS models also predicting strong positive correlations at all supergiant surface gravities (Figures 9 and 10).

In the Milky Way the CaT equivalent width is positively correlated with $\log g$ and M_{bol} . No correlation is seen in the LMC data; however, the SMC sample shows a positive correlation between the CaT equivalent width and M_{bol} .

Ca I: The MARCS models predict a correlation between the equivalent width of the Ca I 6572.0 line and T_{eff} for all but the lowest surface gravities and highest metallicities (e.g., the $\log g = -0.5$ models at Milky Way metallicity and the $\log g = -0.5$ and $\log g = 0.0$ models at LMC metallicity). However, this is not borne out by our observations (Figure 3); the LMC and SMC samples show no significant correlation between Ca I and T_{eff} , while the Milky Way sample shows a moderately strong positive correlation ($r=0.500$) with a borderline $p=0.01$. It is also worth noting that the MARCS models predict a positive correlation between Ca I and T_{eff} at Milky Way metallicity, but a negative correlation at the lower LMC and SMC metallicities, with the Ca I line getting weaker at higher T_{eff} .

Ti I/Fe I Ratio: None of the observed data revealed significant correlations between the Ti I 8518.1/Fe I 8514.1 ratio (Figure 4) and RSG physical properties. By contrast, the MARCS models predict significant negative correlations between this ratio and T_{eff} for all $\log g$ values at Milky Way metallicity, while the LMC and SMC metallicity models show significant negative correlations at particular values of $\log g$ ($\log g = 0.0$ in the LMC and $\log g = -0.5, 0.0,$ and 1.0 in the SMC).

Ti I Sum: None of the observed samples - at Milky Way, LMC, or SMC metallicity - show any evidence for statistically significant correlations between the sum of the Ti I line (Figure 5) equivalent widths and any RSG physical properties.

The Milky Way metallicity MARCS models predict no statistically significant correlation between Ti I EW and T_{eff} . However, in the LMC the Ti I sum showed a strong positive correlation with T_{eff} for the $\log g = 0.0$ models only ($r=0.997, p=0.00186$), and the SMC models showed a strong negative correlation with T_{eff} at $\log g = -0.5$ ($r=-0.933, p=0.00071$) and a strong positive correlation at $\log g = 0.5$ ($r=0.879, p=0.00404$).

Fe I Sum: Our observed Milky Way and SMC samples show no correlation between the sum of the Fe I line (Figure 6) equivalent widths and any RSG physical properties; however, the LMC sample shows evidence of a positive correlation between the Fe I sum and T_{eff} . Both of these results are also at odds with the predictions of the MARCS models, which only predict a significant positive correlation between Fe I and T_{eff} for Milky Way supergiants with $\log g = 1.0$ ($r=0.965, p=0.0001$) and a significant *negative* correlation between Fe I and T_{eff} for SMC supergiants with $\log g = 0.5$ and 1.0 ($r=-0.972, p=0.00005$ and $r=-0.975, p=0.00004$, respectively).

Ca II 3-D Plots: The CaT equivalent width showed the most promise in our observed data as an atomic line diagnostic of T_{eff} ; however, this feature is also well-known as a potential diagnostic of $\log g$ and luminosity, calling the degeneracy of its T_{eff} correlation into question. To further examine this we created 3D plots for our observed data from all three host galaxies with T_{eff} , $\log g$, and Ca II EW (see Figure 7) as the respective x, y, and z axes. ² These data were then fitted with linear and quadratic planes of best fit. The full suite of correlation coefficients for the data in the 3D plots is given in Table 9, and equations for the linear and quadratic best fits are given in Table 10. The linear plane best fit

equation is $Z = Ax + By + C$, while the quadratic plane fit is $Z = Ax + By + Cxy + Dx^2 + Ey^2 + F$.

4. DISCUSSION AND FUTURE WORK

In light of the small sample sizes used in this work (25 stars in the Milky Way sample, 16 in the LMC, and 17 in the SMC) we are cautious about over-interpreting the statistical results drawn from our data. However, it is still interesting to examine areas where our observations and model results agree or diverge from each other and from past work, and to consider potential physical explanations for why this may be and the implications for future work.

Our observed spectra show a strong positive correlation ($r = 0.755, p = 0.00001$) between CaT and T_{eff} for MW RSGs, in agreement with the predictions of the MARCS stellar atmosphere models. However, it is difficult to discern whether this is primarily a consequence of T_{eff} or $\log g$ effects on the CaT absorption features and surrounding continuum. In the MW there is a significant correlation ($r = 0.549, p = 0.0082$) between T_{eff} and $\log g$, with cooler stars having lower surface gravities (an unsurprising consequence of the effect that a decreasing T_{eff} and constant or increasing M_{bol} will have on the stellar radii), and both $\log g$ and M_{bol} are positively correlated with the CaT sum (see Table 9). Figure 7 compares the CaT equivalent width, T_{eff} , and $\log g$ of our Milky Way stars in 3-D space, along with the best quadratic plane fit to the sample, but - as also noted by previous work - it is unclear which physical property is primarily responsible for driving the evolution of CaT in RSG spectra.

We also do *not* see any correlation between CaT and T_{eff} in either the LMC or SMC observations. While this suggests that metallicity may also play a role in the evolution of the CaT with stellar properties (in agreement with previous work that found a metallicity dependence in the CaT equivalent width for supergiants (e.g. [Armandroff & Da Costa 1991](#); [Ginestat et al. 2016](#); [Mallik 1996](#)) this is at odds with the predictions of the MARCS models, which predict a strong correlation between CaT and T_{eff} at all of the model metallicities. The models do, however, predict an expected overall decrease in the strength of the CaT with metallicity. Figures 7-9 compare the MARCS models and observed data, highlighting the decrease in EW with metallicity as well as comparing the EWs predicted by the models to those observed in the data. Note that [Dorda et al. \(2016b\)](#) also directly compare LMC- and SMC-metallicity MARCS model equivalent widths to T_{eff} (though their data span a broader T_{eff} range of 3300-4500 K to better encom-

² The base code to make the 3D plots can be found at <https://gist.github.com/amroamroamro/1db8d69b4b65e8bc66a6>

pass the warmer F-, G-, and K-type supergiants in their observed sample) and find similar results.

Our observed data also blend a range of surface gravities that sample the lower end of RSG surface gravities (the mean $\log g$ of the MW, LMC, and SMC samples is 0.15, -0.275 , AND -0.247 respectively) while the models with different $\log g$ are considered separately. If we combine the results from the MARCS models across *all* surface gravities, the correlations between CaT and T_{eff} get weaker in the Milky Way ($r=0.467$, $p=0.007$) and LMC ($r=0.712$, $p=0.0004$), while the SMC data fails to satisfy our $p < 0.01$ significance threshold ($r=0.356$, $p=0.046$). Considering these results, it is possible that decreased metallicity combined with a mix of surface gravities in our observed samples could contribute to the lack of statistically robust correlation between CaT and T_{eff} in the LMC and SMC data.

Quadratic best fits to the CaT EW, T_{eff} and $\log g$ data in 3D space show a stronger relationship between the three parameters for the lowest T_{eff} and $\log g$ values. The CaT EW is consistently high at high $\log g$ values (≥ 0.6) for all values of T_{eff} , but decreases nearly linearly with $\log g$ at low T_{eff} . Above $T_{\text{eff}} \geq 3750$ K, the relationship between EW and $\log g$ becomes more complex. By comparison, both the LMC and SMC quadratic best fits in 3D show a “concave” shape, with the evolution of CaT as a function of $\log g$ and T_{eff} that is hard to quantify and not well-fit by a linear relation (for example, both high $T_{\text{eff}} + \text{low } \log g$ and low $T_{\text{eff}} + \text{high } \log g$ correspond to CaT EW minimums).

The relationships are simplified (but also more poorly fit) in linear plane best fits to the data, given in Table 10. In this case the MW and LMC results broadly align with predictions from [Ginestat et al. \(2016\)](#) asserting that the intensity of the CaT is correlated with $\log g$, but the SMC does not, suggesting a more complex relationship for this sample. [Erdelyi-Mendes & Barbu \(1990\)](#) concluded that at high metallicity Ca II was inversely related to $\log g$; as the SMC has the lowest metallicity of our sample it suggests that this difference could in part be attributable to changes in this relationship as a function of metallicity.

The [Dorda et al. \(2016a\)](#) sample consisted of early G to M3 stars, with a small sample of later-type M stars, as it was thought that the TiO band would significantly erode the continuum in the latest M type stars and make reliable EW measurements difficult beginning at a spectral type of M0. However, as found both by [Ginestat et al. \(2016\)](#) and this work, the stronger TiO band at later spectral types (corresponding to cool T_{eff} , e.g. [Levesque et al. 2005](#); [Taberner et al. 2018](#)) reliably corresponds to a decrease in the local continuum, and

a subsequent apparent weakening of the CaT, in agreement with the evolution of the CaT seen at warmer T_{eff} . This effect therefore improves rather than weakens the utility of the CaT as a T_{eff} diagnostic. For a direct comparison between the models results and the MW, LMC, and SMC results see Figures 8-10.

Moving beyond the CaT feature, it is interesting to note that there is no correlation in any of our observed data between Ca I or the Ti/Fe ratio and any RSG physical properties, at odds with what the models predict. Beyond that, most of the observed *and* model samples predict no correlation between the sum of the Ti I or Fe I absorption features and the physical properties of RSGs, with a few noted exceptions. For example, the observed LMC spectra show a positive correlation between the Fe I sum and T_{eff} . However, this is at odds with the predictions of the MARCS stellar evolution models, which only predict correlations between Fe I and T_{eff} for the highest $\log g$ models (notably higher than the average $\log g$ of our observed RSGs), and is almost certainly a consequence of small number statistics in our 16-star LMC sample. Still, since [Dorda et al. \(2016a\)](#) predict a strong correlation between Ti I and Fe I and spectral type for cool supergiants - which we would expect to extend to a correlation between these features and T_{eff} and be observable even in a small sample - it is worth considering some of the physical phenomena that may impact the formation and evolution of these lines in RSG spectra.

Our MARCS model results do not highlight Ti I and Fe I as robust diagnostic lines for M-type RSGs; however, these models also assume LTE. How might non-LTE conditions affect these predictions? [Bergemann et al. \(2012\)](#) studied individual RSGs to determine the impact of non-LTE on Ti I and Fe I spectral features. They found that the significance of non-LTE corrections was dependent on T_{eff} , metallicity, and $\log g$, noting that for both Ti I and Fe I, non-LTE corrections in order to align results with observations were lower, or near zero, at lower temperatures - $3400 \text{ K} \geq T_{\text{eff}} \leq 3800 \text{ K}$. At higher temperatures, the formation of Fe I lines remains largely unaffected by non-LTE, while the Ti I line does show some variation, with Ti I EWs underestimated by LTE as compared to non-LTE models. However, for M-type RSGs non-LTE effects on these lines do not play a significant role and as such cannot be considered a variable for the disagreements between the observed data and the models.

As these are all neutral lines, it is also worth considering the excitation potential of these features. Both [Dorda et al. \(2016a\)](#) and our models predict a relationship between Fe I and T_{eff} and between Ti I and T_{eff} ,

with Dorda et al. (2016a) arguing that this is due to their low excitation potentials (6.82 eV for Ti I, 7.87 eV for Fe I), thus rendering the neutral abundances of these elements particularly sensitive to T_{eff} . However, while this reasoning is robust for warmer stars it breaks down for M-type RSGs. At these low temperatures ($\lesssim 4000$ K) photoionization is no longer the primary means of producing Ti II and Fe II, and instead collision becomes the dominant means of excitation (for more discussion see Bergemann et al. 2012). This decouples the Ti I/Ti II and Fe I/Fe II fractions from T_{eff} in the cool and low-density atmospheres of RSGs. Taken as a whole, the Ti I and Fe I absorption features are not effective diagnostics of T_{eff} for the coolest RSGs (a result in agreement with Dorda et al. (2016b)’s figures 7 and 8, which show a weak correlation between these features and spectral type for the M0-M3 stars in their sample).

The Ca I absorption feature remains a puzzle. The MARCS models predict a positive correlation between Ca I EW and T_{eff} at Milky Way metallicity, but a *negative* correlation for SMC metallicities and the higher surface gravity LMC models. The latter is what would naively be expected based simply on the evolution of the CaT absorption feature: as the Ca II abundance (and the CaT EW increases), we would expect a corresponding decrease in the Ca I abundance and EW. It is unclear why this is predicted at lower metallicities (and higher surface gravities) but not at solar metallicity. It is possible that at higher metallicities the Ca I abundance is high enough to saturate, resulting in a non-linear evolution of the Ca I absorption feature at higher metallicities. As in the case of Ti and Fe, the relative contributions from photoionization and collisional excitation could also play a role. Finally, none of these

expected correlations appear in our observed data, suggesting that additional effects (including the impact of non-LTE) could further complicate the formation and evolution of the Ca I with T_{eff} .

While these results are based on only a small sample of M-type RSGs, it is nevertheless important to consider whether these or other atomic lines can be used to directly infer the stars’ physical properties. To take just one example, spectra from *Gaia* span only a narrow wavelength range ($\sim 8450\text{-}8750\text{\AA}$), but this critical regime includes the CaT absorption feature as well as all of the Ti I absorption lines and 7 of the Fe I absorption lines included in this work. Identifying - or excluding - useful T_{eff} diagnostics in this wavelength regime represents a potentially powerful tool for leveraging the wealth of potential RSG data available in current and future *Gaia* data releases (which extends throughout the Milky Way and to the Large and Small Magellanic Clouds), and may make it possible to greatly improve the accuracy of the physical properties determined for these stars.

We would like to thank Trevor Dorn-Wallenstein, Philip Massey, and George Wallerstein for useful discussions regarding this research, as well as the staff of Apache Point Observatory and Las Campanas Observatory for their support in acquiring the observed spectra used in this work. These efforts were supported in part by a fellowship from the Alfred P. Sloan Foundation.

Software: IPython (Pérez & Granger 2007), SciPy (Jones et al. 2001), NumPy (Van Der Walt et al. 2011), IRAF (Tody 1986, 1993), Matplotlib (Hunter 2007) .

Table 1. Sample Stars

Star	Spectral Type	T_{eff}	$\log g$	M_{bol}	OB Assoc.
MW					
BD+59 38	M2 I	3650	0.1	-7.17	Cas OB4
BD+56 595	M1 I	3800	0.4	-6.31	Per OB1-D
BD+57 647	M2 I	3650	0.0	-7.51	Per OB1-D?
BD+59 274	M1 I	3750	0.4	-6.14	Cas OB8/NGC581
BD+59 372	K5-M0 I	3825	0.6	-5.77	Per OB1-A
BD+60 335	M4 I	3525	0.1	-7.05	Cas OB8/NGC663
BD+60 2613	M3 I	3600	-0.7/-0.4	-9.64/8.57	Cas OB5
BD+60 2634	M3 I	3600	-0.1	-7.73	Cas OB5
Case 23	M3 I	3600	0.3	-6.28	Cas OB7

Table 1 continued

Table 1 (*continued*)

Star	Spectral Type	T_{eff}	$\log g$	M_{bol}	OB Assoc.
Case 80	M3 I	3600	0.1	-7.00	Cas OB2
Case 81	M2 I	3700	0.1	-7.19	Cas OB2
HD 14469	M3-4 I	3575	-0.1	-7.64	Per OB1-D
HD 14488	M4 I	3550	-0.3	-8.15	Per OB1-D/NGC884
HD 23475	M2.5 II	3625	—	—	—
HD 35601	M1.5 I	3700	0.2	-6.81	Aur OB1
HD 36389	M2 I	3650	—	—	—
HD 37536	M2 I	3700	0.1	-7.33	Aur OB1
HD 42475	M1 I	3700	-0.1	-7.76	Gem OB1
HD 42543	M0 I	3800	0.0	-7.55	Gem OB1
HD 44537	M0 I	3750	—	—	—
HD 219978	M1 I	3750	0.4	-6.44	Cep OB3
HD 236697	M1.5 I	3700	0.4	-6.25	NGC 457
HD 236871	M2 I	3625	0.2	-6.80	Cas OB8
HD 236915	M2 I	3650	0.3	-6.40	Per OB1-A
W Per	M4.5 I	3550	0.1	-7.09	Per OB1-D?
LMC					
LMC 064048	M2.5 I	3500	-0.2	-7.81	...
LMC 109106	M2.5 I	3550	-0.2	-7.89	...
LMC 116895	M0 I	3750	-0.2	-8.10	...
LMC 141430	M1 I	3700	-0.3	-8.55	...
LMC 142202	M1.5 I	3650	-0.3	-8.36	...
LMC 146126	K5 I	3875	-0.2	-8.62	...
LMC 061753	M2 I	3600	0.0	-7.80	...
LMC 170452	M2.5 I	3550	-0.5	-8.67	...
WOH S274	M1.5 I	3650	0.0	-8.24	...
HV 12802	M1 I	3700	-0.5	-8.28	...
LMC 170079	M2 I	3625	-0.5	-8.80	...
LMC 054365	M2.5 I	3525	-0.2	-7.88	...
LMC 068125	M4 I	3475	-0.3	-8.21	...
LMC 135720	M4.5 I	3425	-0.4	-8.38	...
LMC 174714	M1.5 I	3625	-0.3	-8.39	...
LMC 175746	M3 I	3500	-0.3	-8.35	...
SMC					
SMC 005092	M2 I	3475	-0.4	-8.48	...
SMC 008930	M0 I	3625	-0.3	-8.38	...
SMC 018136	M0 I	3575	-0.4	-8.76	...
SMC 020133	M0 I	3625	-0.3	-8.39	...
SMC 025879	M0 I	3700	-0.3	-8.44	...
SMC 050840	M1 I	3625	-0.2	-8.12	...
SMC 060447	K2 I	3900	0.1	-7.37	...

Table 1 *continued*

Table 1 (*continued*)

Star	Spectral Type	T_{eff}	$\log g$	M_{bol}	OB Assoc.
SMC 069886	M2 I	3750	-0.3	-8.76	...
SMC 078282	M3 I	3600	-0.5	-9.23	...
SMC 055275	M2 I	3650	0.0	-7.88	...
SMC 056389	M2 I	3675	-0.5	-8.56	...
J00534794-7202095	M3 I	3575	-0.5	-8.77	...
SMC 011709	K5-M0 I	3725	-0.1	-7.93	...
SMC 046497	K5-M0 I	3700	-0.2	-8.30	...
SMC 049478	K5-M0 I	3700	-0.3	-8.49	...
SMC 052334	K5-M0 I	3675	0.0	-7.82	...
SMC 056732	K5-M0 I	3725	0.0	-7.66	...

Table 3. Ca I and CaT Equivalent Widths

Star	6572	8498	8542	8662
Milky Way				
BD+59 38	0.311	2.14	3.61	3.30
BD+56 595	0.38	2.50	5.00	4.11
BD+57 647	0.388	2.19	4.61	3.79
BD+59 274	0.363	2.36	4.79	4.25
BD+59 372	0.350	2.37	5.01	3.96
BD+60 335	0.378	2.28	4.11	3.40
BD+60 2613	0.304	1.92	2.35	2.59
BD+60 2634	0.314	2.08	2.59	3.16
Case 23	0.356	2.31	3.63	3.76
Case 80	0.359	2.26	3.84	3.69
Case 81	0.373	2.38	4.48	4.00
HD 14469	0.347	2.28	3.67	3.32
HD 14488	0.295	2.07	1.76	2.34
HD 23475	0.370	2.25	4.25	3.42
HD 35601	0.381	2.36	4.48	3.81
HD36309	0.395	2.47	3.83	3.69
HD 37536	0.369	2.30	4.17	3.55
HD 42475	0.343	2.40	4.64	3.87
HD 42543	0.379	2.23	5.21	3.74
HD 44537	0.402	2.85	5.08	4.49
HD 219978	0.376	2.37	5.29	4.23
HD 236697	0.380	2.48	5.23	4.18
HD 236871	0.368	2.10	4.57	3.74
HD 236915	0.370	2.33	4.56	3.81

Table 3 continued

Table 2. Measured Absorption Features and Upper and Lower Bounds for Local Continuum

Wavelength (Å)	Chem. Species	Min. (MW)	Max. (MW)	Min. (LMC)	Max. (LMC)	Min. (SMC)	Max. (SMC)
6572.0	Ca I	6571.0	6572.35	6572.35	6573.48	6571.91	6573.43
8498.0	Ca II	8492.40	8503.55	8494.5	8501.00	8495.00	8501.50
8514.1	Fe I	8513.40	8514.80	8513.28	8514.97	8513.19	8514.64
8518.1	Ti I	8516.60	8520.25	8517.40	8518.96	8517.68	8619.03
8542.0	Ca II	8533.35	8551.50	8533.5	8547.20	8533.75	8547.40
8582.0	Fe I	8581.73	8583.40	8581.274	8583.745	8581.24	8583.60
8611.0	Fe I	8609.95	8611.45	8611.085	8612.740	8611.03	8612.30
8662.0	Ca II	8653.00	8669.50	8655.30	8666.50	8655.50	8666.50
8679.4	Fe I	8679.2	8680.3	8678.0	8679.4	8678.6	8679.4
8683.0	Ti I	8681.3	8684.7	8681.6	8683.7
8688.5	Fe I	8687.0	8689.3	8687.6	8689.5	8685.6	8690.7
8692.0	Ti I	8690.4	8693.0
8710.2	Fe I	8709.8	8710.4	8709.9	8711.2	8709.9	8711.7
8712.8	Fe I	8711.0	8713.5	8711.6	8713.8	8712.0	8715.4
8730.5	Ti I	8728.2	8730.5
8757.0	Fe I	8754.8	8759.6	8756.3	8757.9	8756.5	8758.8
8793.2	Fe I	8791.4	8795.5	8792.6	8794.2	8792.4	8794.2
8805.0	Fe I	8802.6	8805.7	8804.0	8805.8	8804.0	8805.9
8824.0	Fe I	8823.0	8825.3	8823.2	8825.6	8823.4	8825.7
8838.0	Fe I	8837.7	8838.6	8836.7	8840.3	8837.3	8840.6

Table 3 (*continued*)

Star	6572	8498	8542	8662
W Per	0.291	2.13	2.95	2.85
LMC				
LMC 064048	0.377	2.367	4.611	3.619
LMC 109106	0.4133	2.59	4.72	4.50
LMC 116895	0.425	2.59	4.92	4.40
LMC 141430	0.383	2.21	3.64	3.21
LMC 142202	0.381	2.44	4.23	4.01
LMC 146126	0.389	2.40	3.95	3.63
LMC 061753	0.338	1.83	4.02	3.07
LMC 170452	0.285	2.03	2.93	3.27
WOH S274	0.430	2.38	3.73	3.71
HV 12802	0.397	2.24	3.11	3.30
LMC 170079	0.366	2.32	3.61	3.50
LMC 054365	0.410	2.42	4.65	4.03
LMC 068125	0.368	2.21	3.23	3.22
LMC 135720	0.300	1.99	2.41	2.50
LMC 174714	0.430	2.07	3.50	3.11
LMC 175746	0.347	2.27	3.60	3.55

Table 3 continued

Table 3 (*continued*)

Star	6572	8498	8542	8662
SMC				
SMC 005092	0.385	1.53	2.75	2.79
SMC 008930	0.353	1.92	3.76	3.62
SMC 018136	0.360	2.27	4.16	3.38
SMC 020133	0.334	1.89	3.81	3.29
SMC 025879	0.312	2.06	4.04	3.71
SMC 050840	0.365	2.11	4.32	3.56
SMC 060447	0.36	2.01	4.37	3.54
SMC 069886	0.343	1.44	2.30	2.78
SMC 078282	0.305	1.51	2.85	3.17
SMC 055275	0.355	1.93	4.00	3.088
SMC 056389	0.334	1.92	3.42	3.15
J00534794-7202095	0.322	1.87	3.25	3.23
SMC 011709	0.355	2.08	4.21	3.72
SMC 046497	0.352	1.97	3.86	3.31
SMC 049478	0.352	1.96	3.87	3.04
SMC 052334	0.346	1.98	4.28	3.51
SMC 056732	0.343	1.97	4.31	3.41

Table 4. Fe I Equivalent Widths

Star	8514.1	8582.0	8611.0	8679.4	8688.5	8710.2	8712.8	8757.0	8793.2	8805.0	8824.0	8838.0
Milky Way												
BD+59 38	0.319	0.148	0.100	0.034	0.453	0.025	0.470	0.443	0.325	0.282	0.477	0.052
BD+56 595	0.299	0.192	0.146	0.051	0.444	0.030	0.493	0.454	0.343	0.267	0.424	0.069
BD+57 647	0.320	0.171	0.119	0.039	0.488	0.022	0.471	0.516	0.399	0.243	0.476	0.052
BD+59 274	0.306	0.171	0.132	0.057	0.408	0.029	0.406	0.388	0.299	0.241	0.373	0.060
BD+59 372	0.306	0.185	0.140	0.061	0.413	0.031	0.409	0.454	0.308	0.212	0.380	0.064
BD+60 335	0.264	0.158	0.108	0.038	0.401	0.025	0.449	0.454	0.303	0.259	0.455	0.065
BD+60 2613	0.251	0.262	0.235	0.087	0.508	0.017	0.379	0.498	0.357	0.279	0.439	0.066
BD+60 2634	0.236	0.169	0.092	0.038	0.492	0.029	0.411	0.391	0.301	0.224	0.391	0.031
Case 23	0.305	0.160	0.119	0.046	0.498	0.033	0.450	0.425	0.331	0.266	0.426	0.045
Case 80	0.297	0.211	0.118	0.050	0.496	0.029	0.480	0.400	0.292	0.241	0.385	0.047
Case 81	0.330	0.186	0.152	0.053	0.563	0.033	0.489	0.457	0.333	0.271	0.423	0.047
HD 14469	0.251	0.155	0.103	0.047	0.603	0.033	0.415	0.484	0.296	0.281	0.468	0.048
HD 14488	0.238	0.144	0.069	0.034	0.453	0.023	0.091	0.452	0.246	0.243	0.460	0.049
HD 23475	0.317	0.191	0.155	0.068	0.361	0.027	0.339	0.353	0.242	0.247	0.434	0.067
HD 35601	0.319	0.179	0.179	0.042	0.459	0.035	0.502	0.450	0.294	0.284	0.418	0.030
HD 36389	0.301	0.194	0.128	0.050	0.411	0.035	0.546	0.466	0.266	0.279	0.433	0.047

Table 4 continued

Table 4 (continued)

Star	8514.1	8582.0	8611.0	8679.4	8688.5	8710.2	8712.8	8757.0	8793.2	8805.0	8824.0	8838.0
HD 37536	0.288	0.194	0.124	0.040	0.390	0.027	0.456	0.457	0.278	0.287	0.342	0.033
HD 42475	0.253	0.192	0.096	0.031	0.602	0.018	0.535	0.546	0.353	0.302	0.463	0.040
HD 42543	0.275	0.182	0.114	0.026	0.579	0.029	0.463	0.542	0.379	0.338	0.472	0.052
HD 44537	0.294	0.208	0.150	0.038	0.541	0.034	0.470	0.590	0.414	0.372	0.460	0.044
HD 219978	0.312	0.188	0.155	0.061	0.496	0.038	0.484	0.442	0.287	0.270	0.417	0.077
HD 236697	0.305	0.224	0.138	0.062	0.482	0.031	0.441	0.402	0.277	0.233	0.412	0.083
HD 236871	0.303	0.167	0.124	0.046	0.518	0.033	0.476	0.415	0.351	0.260	0.435	0.065
HD 236915	0.302	0.207	0.117	0.059	0.496	0.024	0.423	0.379	0.235	0.225	0.393	0.077
W Per	0.243	0.167	0.079	0.021	0.706	0.012	0.398	0.562	0.270	0.306	0.459	0.061
LMC												
LMC 064048	0.323	0.204	0.266	0.047	0.655	0.182	0.248	0.288	0.292	0.554	0.605	0.964
LMC 109106	0.356	0.243	0.328	0.065	0.712	0.150	0.290	0.333	0.310	0.343	0.690	0.738
LMC 116895	0.320	0.213	0.353	0.064	0.747	0.187	0.333	0.515	0.336	0.684	0.784	1.031
LMC 141430	0.275	0.359	0.309	0.045	0.706	0.167	0.323	0.513	0.335	0.597	0.720	0.799
LMC 142202	0.324	0.407	0.334	0.036	0.751	0.133	0.377	0.499	0.371	0.621	0.730	0.779
LMC 146126	1.103	0.446	0.501	0.026	1.100	0.170	0.4139	0.609	0.475	0.803	1.001	0.763
LMC 061753	0.897	0.368	0.361	0.085	0.974	0.283	0.400	0.566	0.449	0.746	1.438	0.725
LMC 170452	0.226	0.340	0.349	0.067	1.017	0.129	0.425	0.351	0.247	0.562	0.714	0.650
WOH S274	0.314	0.455	0.386	0.067	1.153	0.141	0.491	0.480	0.271	0.667	0.832	0.689
HV 12802	0.618	0.401	0.400	0.055	1.119	0.146	0.459	0.468	0.259	0.668	0.880	0.700
LMC 170079	0.290	0.366	0.253	0.054	0.675	0.161	0.239	0.296	0.298	0.591	0.682	0.680
LMC 054365	0.333	0.452	0.323	0.058	0.728	0.153	0.236	0.478	0.311	0.636	0.709	0.767
LMC 068125	0.290	0.289	0.227	0.048	0.597	0.136	0.198	0.251	0.242	0.467	0.539	0.644
LMC 135720	0.252	0.218	0.190	0.035	0.600	0.092	0.154	0.222	0.162	0.476	0.633	0.701
LMC 174714	0.865	0.382	0.405	0.036	1.205	0.153	0.423	0.491	0.438	0.720	0.938	0.815
LMC 175746	0.312	0.446	0.279	0.052	0.379	0.156	0.278	0.292	0.289	0.565	0.683	0.727
SMC												
SMC 005092	0.255	0.332	0.374	0.038	1.056	0.149	0.417	0.376	0.246	0.319	0.718	0.717
SMC 008930	0.329	0.238	0.357	0.047	0.725	0.157	0.454	0.319	0.225	0.300	0.687	0.626
SMC 018136	0.332	0.439	0.387	0.039	0.694	0.139	0.257	0.325	0.212	0.297	0.760	0.586
SMC 020133	0.227	0.397	0.369	0.038	0.616	0.116	0.385	0.326	0.241	0.277	0.738	0.510
SMC 025879	0.286	0.336	0.357	0.035	0.663	0.168	0.294	0.327	0.229	0.277	0.694	0.631
SMC 050840	0.328	0.251	0.328	0.032	0.666	0.119	0.247	0.304	0.199	0.288	0.743	0.522
SMC 060447	0.317	0.258	0.324	0.056	0.628	0.124	0.263	0.303	0.214	0.249	0.699	0.652
SMC 069886	0.190	0.094	0.263	0.061	0.459	0.183	0.104	0.298	0.176	0.283	0.649	0.539
SMC 078282	0.343	0.215	0.292	0.059	0.583	0.103	0.176	0.275	0.176	0.255	0.617	0.477
SMC 055275	0.229	0.254	0.333	0.044	0.656	0.145	0.191	0.361	0.235	0.291	0.634	0.691
SMC 056389	0.318	0.396	0.376	0.055	0.731	0.124	0.450	0.349	0.257	0.313	0.780	0.571
J00534794-7202095	0.301	0.193	0.341	0.040	0.665	0.137	0.451	0.325	0.217	0.256	0.697	0.547
SMC 011709	0.309	0.263	0.345	0.046	0.704	0.133	0.476	0.309	0.264	0.372	0.722	0.563
SMC 046497	0.295	0.237	0.313	0.025	0.643	0.122	0.337	0.304	0.222	0.284	0.820	0.508

Table 4 continued

Table 4 (*continued*)

Star	8514.1	8582.0	8611.0	8679.4	8688.5	8710.2	8712.8	8757.0	8793.2	8805.0	8824.0	8838.0
SMC 049478	0.246	0.371	0.386	0.040	1.032	0.117	0.385	0.499	0.205	0.306	0.813	0.590
SMC 052334	0.290	0.354	0.344	0.044	0.660	0.121	0.364	0.327	0.217	0.285	0.747	0.504
SMC 056732	0.327	0.222	0.310	0.038	0.617	0.115	0.253	0.284	0.197	0.271	0.796	0.614

Table 5. Ti I Equivalent Widths

Star	8518.1	8683.0	8692.0	8730.5	8734.5
Milky Way					
BD+59 38	0.422	0.497	0.261	0.170	0.345
BD+56 595	0.412	0.430	0.277	0.202	0.305
BD+57 647	0.511	0.582	0.292	0.205	0.305
BD+59 274	0.473	0.434	0.253	0.189	0.285
BD+59 372	0.463	0.422	0.226	0.179	0.274
BD+60 335	0.459	0.536	0.238	0.181	0.348
BD+60 2613	0.367	0.531	0.198	0.123	0.278
BD+60 2634	0.374	0.701	0.287	0.160	0.340
Case 23	0.480	0.453	0.211	0.184	0.348
Case 80	0.459	0.426	0.215	0.181	0.319
Case 81	0.523	0.443	0.268	0.205	0.314
HD 14469	0.395	0.532	0.239	0.199	0.274
HD 14488	0.279	0.443	0.202	0.136	0.333
HD 23475	0.447	0.420	0.247	0.173	0.291
HD 35601	0.508	0.444	0.201	0.199	0.317
HD 36389	0.528	0.493	0.233	0.209	0.346
HD 37536	0.484	0.437	0.185	0.177	0.326
HD 42475	0.474	0.524	0.220	0.148	0.273
HD 42543	0.536	0.567	0.225	0.208	0.328
HD 44537	0.543	0.549	0.293	0.212	0.288
HD 219978	0.491	0.465	0.256	0.192	0.298
HD 236697	0.480	0.481	0.201	0.178	0.312
HD 236871	0.458	0.523	0.257	0.204	0.335
HD 236915	0.453	0.487	0.279	0.190	0.311
W Per	0.412	0.653	0.296	0.187	0.362
LMC					
LMC 064048	0.261	0.319	0.346	0.105	0.274
LMC 109106	0.284	0.339	0.374	0.143	0.283
LMC 116895	0.267	0.342	0.437	0.164	0.273
LMC 141430	0.232	0.280	0.348	0.095	0.247
LMC 142202	0.200	0.335	0.4308	0.118	0.254

Table 5 continued

Table 5 (*continued*)

Star	8518.1	8683.0	8692.0	8730.5	8734.5
LMC 146126	0.055	0.446	0.168	0.134	0.055
LMC 061753	0.373	0.342	0.247	0.100	0.132
LMC 170452	0.153	0.400	0.292	0.171	0.296
WOH S274	0.231	0.346	0.359	0.191	0.279
HV 12802	0.291	0.306	0.334	0.176	0.227
LMC 170079	0.229	0.368	0.367	0.120	0.295
LMC 054365	0.277	0.331	0.344	0.129	0.308
LMC 068125	0.252	0.322	0.344	0.117	0.303
LMC 135720	0.190	0.386	0.463	0.092	0.275
LMC 174714	0.339	0.394	0.439	0.106	0.265
LMC 175746	0.236	0.369	0.378	0.148	0.304
SMC					
SMC 005092	0.297	0.348	0.296	0.017	0.222
SMC 008930	0.206	0.279	0.222	0.071	0.196
SMC 018136	0.222	0.286	0.402	0.112	0.264
SMC 020133	0.193	0.225	0.293	0.074	0.194
SMC 025879	0.173	0.276	0.199	0.040	0.164
SMC 050840	0.222	0.259	0.345	0.078	0.272
SMC 060447	0.216	0.216	0.288	0.015	0.233
SMC 069886	0.118	0.201	0.381	0.020	0.217
SMC 078282	0.245	0.288	0.338	0.011	0.263
SMC 055275	0.223	0.234	0.205	0.016	0.191
SMC 056389	0.179	0.259	0.238	0.039	0.169
J00534794-7202095	0.192	0.296	0.263	0.014	0.210
SMC 011709	0.211	0.265	0.267	0.076	0.187
SMC 046497	0.193	0.250	0.284	0.013	0.212
SMC 049478	0.195	0.229	0.327	0.091	0.213
SMC 052334	0.203	0.260	0.289	0.065	0.218
SMC 056732	0.223	0.249	0.329	0.014	0.228

Table 6. MARCS Model Equivalent Widths

$\log g$	Feature	3300 K	3400 K	3500 K	3600 K	3700 K	3800 K	3900 K	4000 K
Milky Way									
-0.5	Ca II Sum	9.99	10.93	11.7	12.0	12.4	12.7	13.0	13.0
	Ca I 6575.5	0.703	0.871	1.14	1.26	1.30	1.33	1.34	1.32
	Ti I 8520.0	0.536	0.615	0.635	0.631	0.614	0.575	0.536	0.490
	Ti I Sum	2.02	2.23	2.39	2.50	2.54	2.60	2.57	2.47
	Fe I 8516.5	0.716	0.818	0.880	0.920	0.946	0.962	0.970	0.967

Table 6 continued

Table 6 (continued)

$\log g$	Feature	3300 K	3400 K	3500 K	3600 K	3700 K	3800 K	3900 K	4000 K
	Fe I Sum	7.27	8.14	8.49	8.97	9.23	9.70	9.61	9.36
0.0	Ca II Sum	9.95	11.07	12.36	13.57	13.99	14.62	14.93	15.68
	Ca I 6575.5	0.678	0.807	1.07	1.19	1.25	1.28	1.31	1.32
	Ti I 8520.0	0.457	0.533	0.561	0.563	0.516	0.526	0.492	0.451
	Ti I Sum	1.73	1.95	2.13	2.24	2.27	2.33	2.35	2.28
	Fe I 8516.5	0.647	0.760	0.828	0.871	0.900	0.919	0.928	0.928
	Fe I Sum	6.49	7.40	7.77	8.15	8.44	8.73	8.80	8.87
0.5	Ca II Sum	6.85	7.43	7.97	8.45	8.79	9.11	9.29	9.81
	Ca I 6575.5	0.650	0.694	0.953	1.10	1.19	1.27	1.31	1.30
	Ti 8520.0	0.386	0.457	0.488	0.496	0.473	0.473	0.443	0.411
	Ti I Sum	1.44	1.63	1.74	2.51	2.90	3.08	3.24	1.98
	Fe I 8516.5	0.580	0.693	0.762	0.810	0.844	0.865	0.879	0.886
	Fe I Sum	5.64	6.23	6.76	7.28	7.70	7.92	7.99	7.94
1.0	Ca II Sum	6.62	7.19	7.71	8.22	8.73	9.09	9.44	9.528
	Ca I 6575.5	0.622	0.683	0.828	1.04	1.14	1.20	1.24	1.24
	Ti 8520.0	0.324	0.389	0.421	0.432	0.434	0.419	0.401	0.370
	Ti I Sum	1.40	1.57	1.80	1.97	2.11	2.21	2.29	2.29
	Fe I 8516.5	0.523	0.620	0.690	0.741	0.777	0.812	0.822	0.832
	Fe I Sum	3.96	4.43	4.70	4.96	5.20	5.37	5.46	5.50
LMC									
- 0.5	Ca II Sum	7.48	8.28	9.75	10.36	10.84	11.19	11.48	11.50
	Ca I 6575.5	0.134	0.145	0.079	0.130	0.150	0.170	0.178	0.182
	Ti I 8520.0	0.414	0.349	0.322	0.269	0.250	0.231	0.207	0.183
	Ti I Sum	2.279	2.08	2.005	2.12	2.19	2.26	2.29	2.29
	Fe I 8516.5	0.854	0.662	0.569	0.572	0.582	0.584	0.587	0.569
	Fe I Sum	3.898	3.26	3.346	3.386	3.556	3.664	3.68	3.67
0.0	Ca II Sum	6.81	7.90	8.44	8.91	9.41	9.89	10.23	10.54
	Ca I 6575.5	0.657	0.454	0.442	0.309	0.269	0.329	0.316	0.291
	Ti I 8520.0	0.394	0.317	0.282	0.265	0.255	0.203	0.182	0.152
	Ti I Sum	1.83	1.71	1.66	1.71	1.76	1.75	1.77	1.74
	Fe I 8516.5	3.67	3.60	3.53	3.72	3.94	4.016	4.37	3.96
	Fe I Sum	3.67	3.60	3.53	3.72	3.94	4.016	4.37	3.96
0.5	Ca II Sum	6.21	6.63	6.45	7.90	9.50	10.14	10.28	10.71
	Ca I 6575.5	0.689	0.570	0.389	0.254	0.294	0.254	0.240	0.219
	Ti I 8520.0	0.352	0.289	0.246	0.223	0.185	0.168	0.152	0.131
	Ti I Sum	2.22	2.00	1.89	1.85	1.88	1.95	1.99	2.01
	Fe I 8516.5	0.845	0.680	0.556	0.523	0.538	0.546	0.547	0.537
	Fe I Sum	3.53	3.44	3.32	3.24	3.51	3.56	3.66	3.03
1.0	Ca II Sum	5.50	5.95	6.28	6.64	7.25	7.61	7.89	8.02
	Ca I 6575.5	0.096	0.113	0.109	0.096	0.080	0.043	0.052	0.044
	Ti I 8520.0	0.363	0.288	0.224	0.194	0.166	0.133	0.131	0.115

Table 6 continued

Table 6 (*continued*)

$\log g$	Feature	3300 K	3400 K	3500 K	3600 K	3700 K	3800 K	3900 K	4000 K
	Ti I Sum	2.28	1.96	1.77	1.77	1.80	1.80	1.83	1.83
	Fe I 8516.5	0.827	0.661	0.556	0.512	0.488	0.472	0.484	0.491
	Fe I Sum	3.35	3.04	2.88	2.82	2.81	2.87	2.86	2.91
SMC									
-0.5	Ca II Sum	10.84	11.88	12.75	13.58	14.11	14.26	14.29	14.38
	Ca I 6575.5	0.131	0.112	0.091	0.077	0.060	0.046	0.034	0.025
	Ti I 8520.0	0.299	0.243	0.209	0.185	0.164	0.138	0.109	0.087
	Ti I Sum	1.99	1.97	1.96	1.86	1.88	1.88	1.81	1.72
	Fe I 8516.5	0.646	0.534	0.495	0.508	0.512	0.516	0.502	0.488
	Fe I Sum	3.26	3.21	3.24	3.28	3.42	3.37	3.38	3.24
0.0	Ca II Sum	9.13	9.68	10.15	10.86	11.27	11.6	11.67	11.9
	Ca I 6575.5	0.122	0.100	0.087	0.029	0.054	0.044	0.031	0.026
	Ti I 8520.0	0.272	0.225	0.175	0.150	0.124	0.105	0.0878	0.0792
	Ti I Sum	1.35	1.45	1.39	1.38	1.37	1.37	1.33	1.27
	Fe I 8516.5	0.843	0.660	0.562	0.524	0.544	0.549	0.553	0.537
	Fe I Sum	3.58	3.49	3.46	3.58	3.53	3.69	3.75	3.75
0.5	Ca II Sum	7.35	7.85	8.34	8.70	9.12	9.33	9.53	9.77
	Ca I 6575.5	0.115	0.115	0.053	0.067	0.054	0.039	0.020	0.024
	Ti I 8520.0	0.261	0.208	0.157	0.129	0.114	0.089	0.0724	0.0613
	Ti I Sum	1.85	1.72	1.66	1.63	1.66	1.63	1.61	1.55
	Fe I 8516.5	0.1561	0.091	0.0452	0.0205	0.0267	0.0359	0.0329	0.0469
	Fe I Sum	2.33	2.34	2.20	2.17	2.16	2.11	2.07	2.01
1.0	Ca II Sum	6.46	6.36	6.89	7.31	7.59	7.86	7.87	8.05
	Ca I 6575.5	0.096	0.113	0.109	0.096	0.080	0.043	0.052	0.044
	Ti I 8520.0	0.233	0.176	0.149	0.122	0.103	0.0797	0.0608	0.0537
	Ti I Sum	1.51	1.47	1.58	1.51	1.49	1.43	1.35	1.27
	Fe I 8516.5	0.587	0.514	0.453	0.427	0.419	0.427	0.432	0.425
	Fe I Sum	2.84	2.72	2.73	2.62	2.59	2.55	2.52	2.39

Table 7. Correlation and Best-Fit Coefficients - Observations

EW	R1:	P1:	Linear	Linear	Quadratic	Quadratic	Quadratic
	T_{eff} vs EW	T_{eff} vs EW	$A \times 10^{-3}$	B	$A \times 10^{-4}$	$B \times 10^{-2}$	C
Milky Way							
Ca II Sum	0.755	0.00001	14.2	-41.99	-3.6	28.11	-532.2
Ca I 6572.0	0.500	0.01	0.019	-0.3407	-0.09979	0.75	-13.81
Ti I Sum	-0.0115	0.9	-0.02	-1.755	0.0083	-0.0063	2.874
Ti I/Fe I Ratio	0.232	0.3	0.0005	-0.1956	-0.00271	24.76	-385.29
Fe I Sum	0.234	0.261	0.8	0.1800	-0.1071	7.953	-144.4
LMC							

Table 7 continued

Table 7 (*continued*)

EW	R1:	P1:	Linear	Linear	Quadratic	Quadratic	Quadratic
	T_{eff} vs EW	T_{eff} vs EW	$A \times 10^{-3}$	B	$A \times 10^{-4}$	$B \times 10^{-2}$	C
CaT Sum	0.320	0.3	370	-3.76	-1.57	11.8	-211.6
Ca I 6572.0	0.455	0.08	0.20	-0.246	-0.0691	0.520	-9.39
Ti I Sum	-0.508	0.04	-0.70	3.86	-0.00048	0.034	-60.09
Ti I/Fe I Ratio	-0.594	0.05	-1.2	4.927	-0.377	2.63	-44.98
Fe I Sum	0.712	0.002	2.00	-19.98	-0.691	5.73	-111.42
SMC							
CaT Sum	0.344	0.2	4.0	-5.63	-0.1446	1.105	-0.0202
Ca I 6572.0	-0.0847	0.7	-0.02	0.412	0.06027	-0.0446	8.5192
Ti I Sum	-0.490	0.05	-0.6	3.35	0.2461	-0.1876	36.75
Ti I/Fe I Ratio	-0.465	0.06	-0.8	3.52	0.4702	-0.354	67.33
Fe I Sum	-0.3054	0.2	-1.4	9.56	0.5332	-0.407	81.91

Table 8. Correlation and Best-Fit Coefficients - MARCS Models

log g	EW	R1:	P1:	Linear	Linear	Quadratic	Quadratic	Quadratic
		T_{eff} vs EW	T_{eff} vs EW	$A \times 10^{-2}$	B	$A \times 10^{-4}$	B	C
Milky Way								
-0.5	CaT Sum	0.937	0.0002	0.34	-0.5974	-0.04081	-0.03412	-57.97
	Ca I 6575.5	0.780	0.0131	0.05918	-1.0271	-0.01515	0.01985	-22.32
-	Ti I Sum	0.0301	0.939	0.002432	2.2700	-0.02727	0.02053	-36.07
-	Ti I/Fe I Ratio	-0.979	0.000004	-0.04	2.2208	-0.000323	0.00199	-2.29
-	Fe I Sum	0.518	0.153	0.1361	3.7286	-0.07506	0.05782	-101.88
0.0	CaT Sum	0.869	0.0023	0.67	-7.875	-0.1269	0.1022	-186.3
	Ca I 6575.5	0.834	0.0052	0.06	1.275	-0.01383	0.01105	-20.7247
-	Ti I Sum	0.347	0.3598	0.03	1.198	-0.02288	0.01746	-30.97
-	Ti I/Fe I Ratio	-0.980	0.000004	-0.04	2.0135	-0.002211	0.001278	-1.0956
-	Fe I Sum	0.604	0.0850	0.0016	224.74	-0.06842	0.05302	-93.95
0.5	CaT Sum	0.926	0.0003	0.3	-2.664	-0.03986	0.033005	-58.70
	Ca I 6575.5	0.874	0.0048	0.07	-1.541	-0.0149	0.01908	-22.48
-	Ti I Sum	0.409	0.275	0.08988	-1.0564	0.05430	0.04175	-77.40
-	Ti I/Fe I Ratio	-0.974	0.001	-0.0004	1.913	-	-	-
-	Fe I Sum	0.785	0.0203	0.204	-0.4100	-0.06111	0.0481	-86.33
1.0	CaT Sum	0.818	0.0071	0.27	-1.7245	-0.06196	0.04931	-88.34
	Ca I 6575.5	0.888	0.0014	0.07236	-1.6663	-0.01196	0.009721	-18.48
-	Ti I Sum	0.779	0.0134	0.08	-1.0700	-0.02192	0.01731	-31.89
-	Ti I/Fe I Ratio	-0.970	0.00007	-0.027	1.52	-0.00031	0.00199	-2.59
-	Fe I Sum	0.965	0.0001	0.216	-2.95	-0.0092	0.0234	-41.65
LMC								
-0.5	CaT Sum	0.945	0.00039	58.3	-11.16	-0.00096	0.076	-138
	Ca I 6575.5	0.694	0.0561	1.000	-0.2009	0.0000231	-0.00159	2.867
-	Ti I Sum	0.526	0.1805	2.4	1.325	0.00012	-0.0086	17.46
-	Ti I/Fe I Ratio	0.357	0.386	0.00003	90.65	-0.00000989	0.000748	-0.4062

Table 8 continued

Table 8 (continued)

log g	EW	R1:	P1:	Linear	Linear	Quadratic	Quadratic	Quadratic
		T_{eff} vs EW	T_{eff} vs EW	$A \times 10^{-2}$	B	$A \times 10^{-4}$	B	C
0.0	Fe I Sum	0.222	0.5962	1.900	2.851	0.00025	-0.0179	35.68
	CaT Sum	0.983	0.00001	50.70	-9.479	-0.000419	0.0357	-65.17
	Ca I 6575.5	-0.8156	0.01358	-4.3	-0.8156	0.0001309	-0.00989	19.33
	Ti I Sum	0.997	0.00186	0.000004	1.74	0.000000554	-0.00405	9.097
	Ti I/Fe I Ratio	-0.843	0.0086	-3.00	1.51	-0.000847	0.00589	-9.73
0.5	Fe I Sum	0.604	0.079	0.01784	0.0009	0.5647	0.00000254	-0.000957
	CaT Sum	0.926	0.00013	74.30	-18.65	-0.00000842	0.0136	29.83
	Ca I 6575.5	-0.8847	0.00356	-6.300	2.666	0.0000149	-0.0115	22.43
	Ti I Sum	-0.3407	0.409	-1.6	2.562	0.00002027	-0.0149	2946
	Ti I/Fe I Ratio	0.409	0.3142	-0.00005	1.133	0.0000000678	-0.00106	2.729
1.0	Fe I Sum	0.672	0.0680	5.8	1.40	0.000295	-0.0210	40.60
	CaT Sum	0.9917	0.000001	38.05	-6.991	-0.00001579	0.0153	-27.95
	Ca I 6575.5	-0.887	0.0033	-1.1	0.463	-0.00000115	-1.066	-
	Ti I Sum	-0.625	0.0974	-4.1	3.386	0.0000227	-0.0170	33.52
	Ti I/Fe I Ratio	-0.453	0.259	-0.3	1.119	-0.00000012	0.000059	0.955
	Fe I Sum	-0.663	0.0731	-4.9	4.719	0.0000257	-0.0192	38.77
SMC								
-0.5	CaT Sum	0.927	0.00093	0.498	-4.926	-0.0999	0.0779	-137.46
	Ca I 6575.5	-0.994	0.000001	-0.015	0.630	0.000824	-0.000754	1.723
	Ti I Sum	-0.933	0.00071	-0.034	3.113	-0.000319	0.00199	-1.107
	Ti I/Fe I Ratio	-0.912	0.00158	-0.043	2.266	0.000659	-0.00524	11.00
0.0	Fe I Sum	0.458	0.255	0.015	2.765	-0.000736	0.00552	-7.00
	CaT Sum	0.974	0.00004	0.406	-4.0513	0.000436	0.0359	-61.862
	Ca I 6575.5	-0.892	0.00287	-0.0130	0.000216	-0.00170	3.415	-
	Ti I Sum	-0.7132	0.0469	-0.015	1.919	-0.000526	0.00367	-5.054
	Ti I/Fe I Ratio	-0.970	0.000071	-0.0304	1.357	-0.000169	0.000930	-0.886
0.5	Fe I Sum	0.799	0.01732	0.0370	2.257	0.000926	-0.00639	14.543
	CaT Sum	0.983	0.00001	0.342	-3.720	-0.0288	0.244	-41.93
	Ca I 6575.5	-0.9244	0.00102	-0.000104	0.569	0.000133	-0.00115	2.343
	Ti I Sum	0.879	0.00404	-3.300	2.852	0.000477	-0.00381	9.185
	Ti I/Fe I Ratio	0.391	0.330	0.0964	-23.157	0.906	0.670	-1225.411
1.0	Fe I Sum	-0.972	0.00005	-4.600	3.862	0.000107	-0.00120	5.277
	CaT Sum	0.967	0.00009	0.260	-2.204	-0.000179	0.0157	-25.924
	Ca I 6575.5	-0.887	0.0033	-0.011	0.463	-0.000115	0.00753	-1.0659
	Ti I Sum	-0.806	0.0157	-0.033	2.653	-0.000157	0.00739	-11.375
	Ti I/Fe I Ratio	-0.993	0.000001	-0.0402	1.725	-0.0000362	-0.000138	1.244
	Fe I Sum	-0.975	0.00004	-0.050	4.662	0.00000121	-0.000648	4.284

Table 9. 3D CaT Correlation Coefficients

Galaxy	EW	R2:	P2:	R3:	P3:
		EW v. Log_g	EW v. Log_g	EW v. M_{bol}	EW v. M_{bol}
MW	CaT Sum	0.665	0.00030	0.721	0.0002
MW	Ca I 6572.0	0.558	0.0070	0.526	0.0119
MW	Ti I Sum	0.162	0.472	0.1593	0.4789
MW	Fe I Sum	-0.0700	0.757	-0.079	0.727
LMC	CaT Sum	0.443	0.0856	0.4471	0.0825
LMC	Ca I 6572.0	0.427	0.104	0.296	0.266
LMC	Ti I Sum	-0.149	0.5808	0.209	0.438
LMC	Fe I Sum	0.398	0.127	0.018	0.948
SMC	CaT Sum	0.5564	0.0204	0.631	0.0066
SMC	Ca I 6572.0	0.3601	0.156	0.436	0.0799
SMC	Ti I Sum	-0.2147	0.4079	-0.239	0.356
SMC	Fe I Sum	0.0866	0.7411	0.0866	0.741

Table 10. CaT 3D Best Fits

Galaxy	EW	Linear	Linear	Linear	Quad	Quad	Quad	Quad	Quad	Quad
		$A \times 10^{-2}$	B	C	A	B	C	D	$E \times 10^{-4}$	F
MW	CaT Sum	0.8	2.927	20.46	-23.21	0.0358	-8.26	0.0027	-0.0869	-0.0741
LMC	CaT Sum	6572.0	0.308	3.50	-0.580	-219.29	0.128	73.02	-0.022	-0.180
SMC	CaT Sum	-0.02246	3.1687	10.5622	-1485.5	0.7967	-303.03	0.08187	-10.6	-11.340

REFERENCES

- Armandroff, T. E., & Da Costa, G. S. 1991, *AJ*, 101, 4
- Bergemann, M., Kudritzki, R. P., Plez, B., et al. 2012, *ApJ*, 751, 156
- Bernstein, R., Shectman, S. A., Gunnels, S. M., Mochnacki, S., & Athey, A. E. 2003, *Instrument Design and Performance for Optical/Infrared Ground-based Telescopes*, 751, 156
- Cenarro, A. J., Cardiel, N., Gorgas, J., Peletier, R. F., & Vazdekis, A. 2001a, *A & A*, 000
- Cenarro, A. J., Gorgas, J., Cardiel, N., et al. 2001b, *A & A*, 326, 981
- Davies, B., Kudritzki, R.-P., & Figer, D. F. 2010, *MNRAS*, 407, 1203
- Davies, B., Kudritzki, R.-P., Gazak, Z., et al. 2015, *ApJ*, 806, 21
- Davies, B., Kudritzki, R.-P., Plez, B., et al. 2013, *ApJ*, 767, 3
- Dorda, R., Gonzalez-Fernandez, C., & Negueruela, I. 2016a, *A & A*, 595, A105
- Dorda, R., Negueruela, I., Gonzalez-Fernandez, C., & Taberner, H. M. 2016b, *A & A*, 592, A16
- Dyck, H. M., Benson, J. A., van Belle, G. T., & Ridgway, S. T. 1996, *AJ*, 111, 1705
- Erdelyi-Mendes, M., & Barbuy, B. 1990, *A & A*, 241, 176
- Gazak, J. Z., Kudritzki, R., Evans, C., et al. 2015, *ApJ*, 805, 182
- Ginestat, N., Carquilla, J. M., Jäschek, M., & Jäschek, C. 2016, *ApJ*, 108, 359
- Gustafsson, B., A., B. R., Eriksson, K., & Nordlund, A. 1975, *A & A*, 42, 407
- Gustafsson, B., Edvardsson, B., Eriksson, K., et al. 2008, *A & A*, 486, 951
- Hayashi, C., & Hoshi, R. 1961, *PASJ*, 13, 450
- Humphreys, R. M., & McElroy, D. B. 1984, *ApJ*, 284, 565

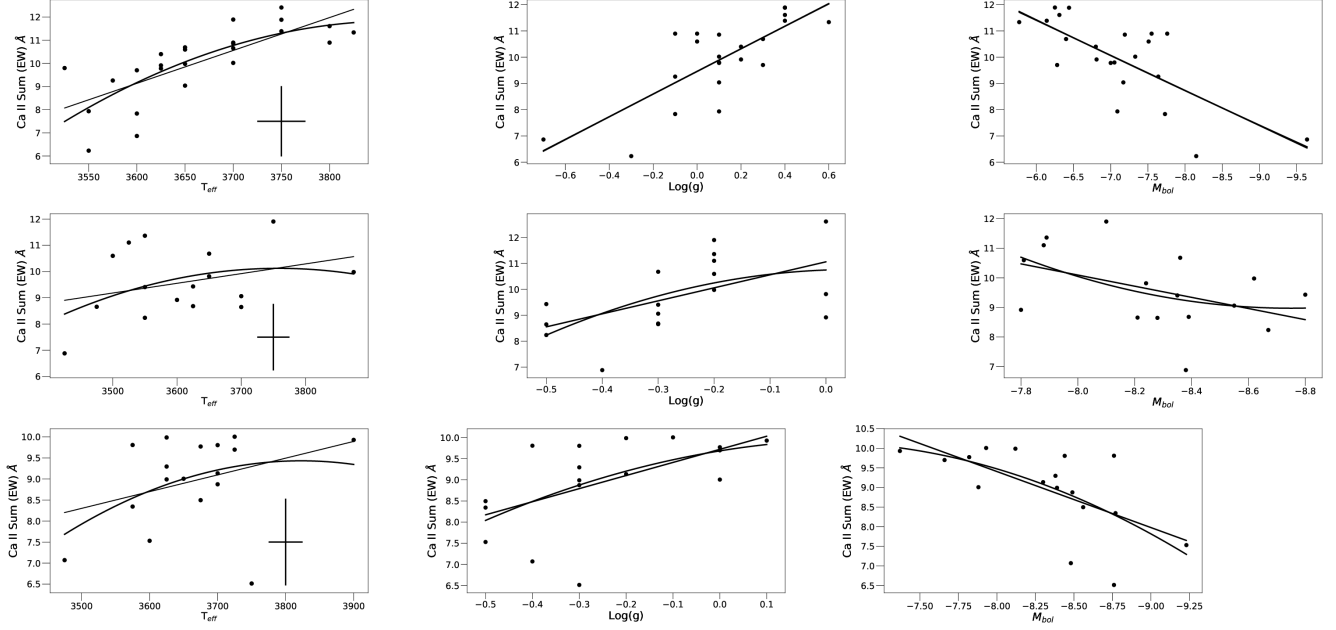


Figure 2. CaT EWs (points) measured in our MW (left), LMC (center), and SMC (bottom) samples, compared to the stars' T_{eff} (left), $\log g$ (center), and M_{bol} (right). For each dataset we have plotted linear and quadratic best fits (solid lines). Systematic error bars for our EW measurements (this work) and errors on the stars' physical properties as given in [Levesque et al. \(2005\)](#) are indicated by crosses (left).

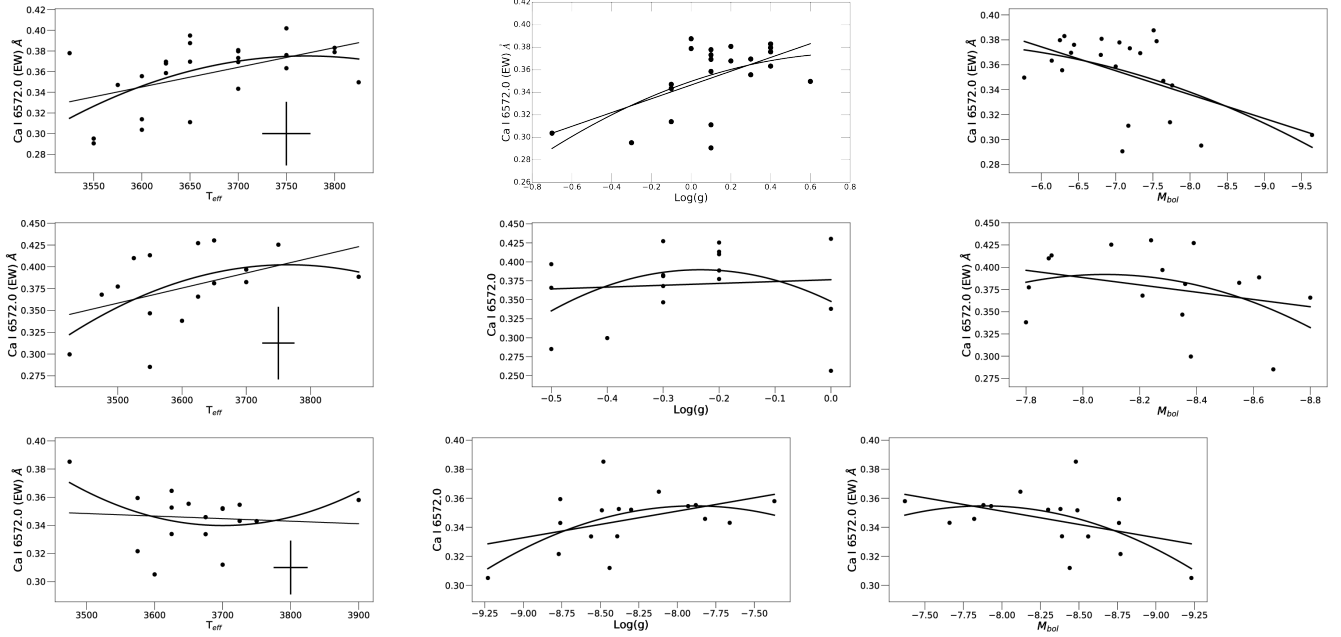


Figure 3. As in Figure 2, but for the Ca I 6572Å absorption feature.

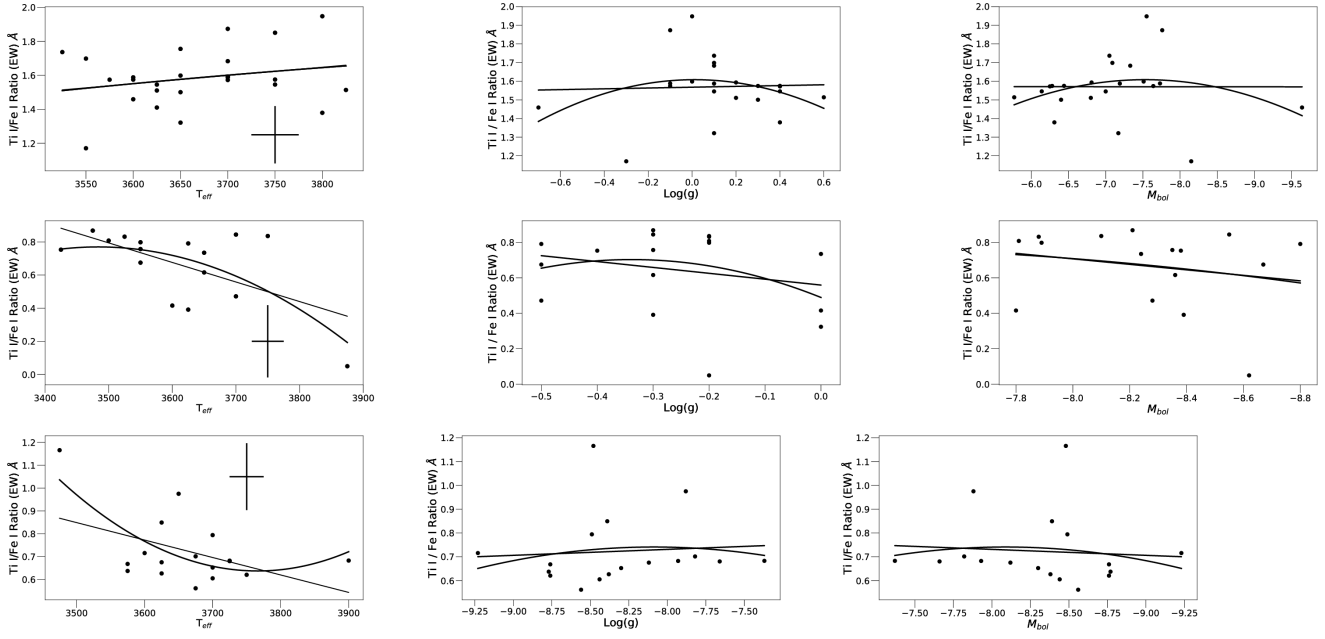


Figure 4. As in Figure 2, but for the ratio of the Ti I 8518Å/Fe II 8514Å absorption features.

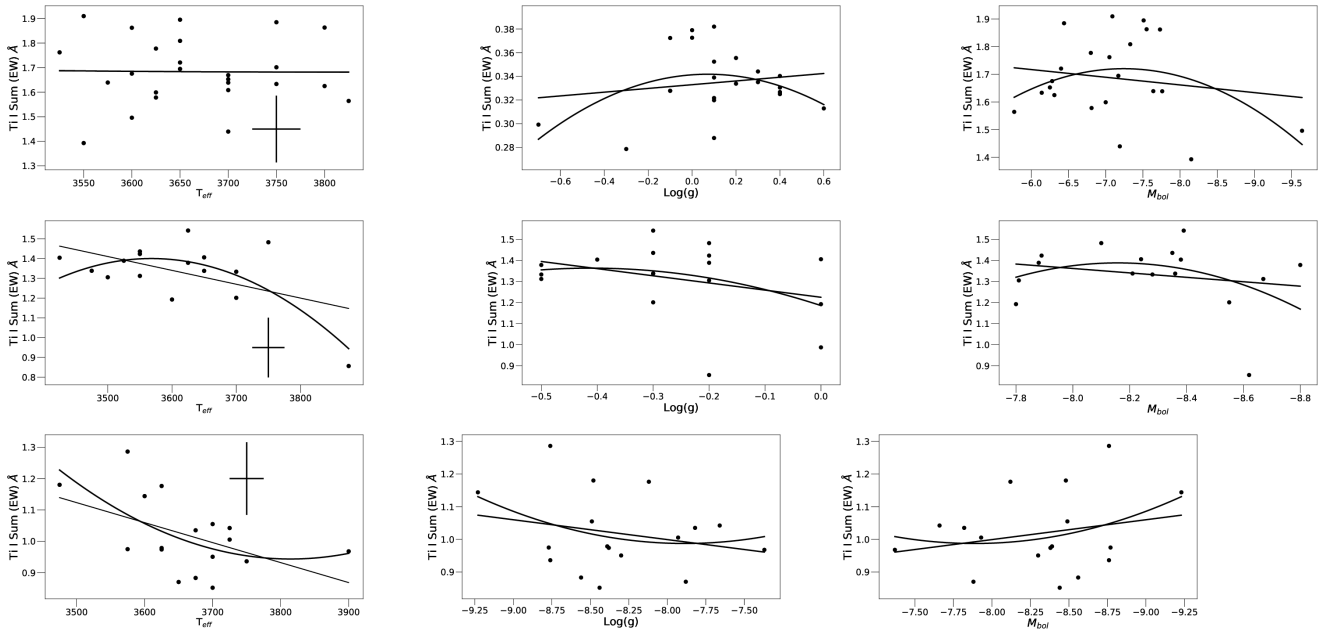


Figure 5. As in Figure 2, but for the sum of the Ti I absorption features.

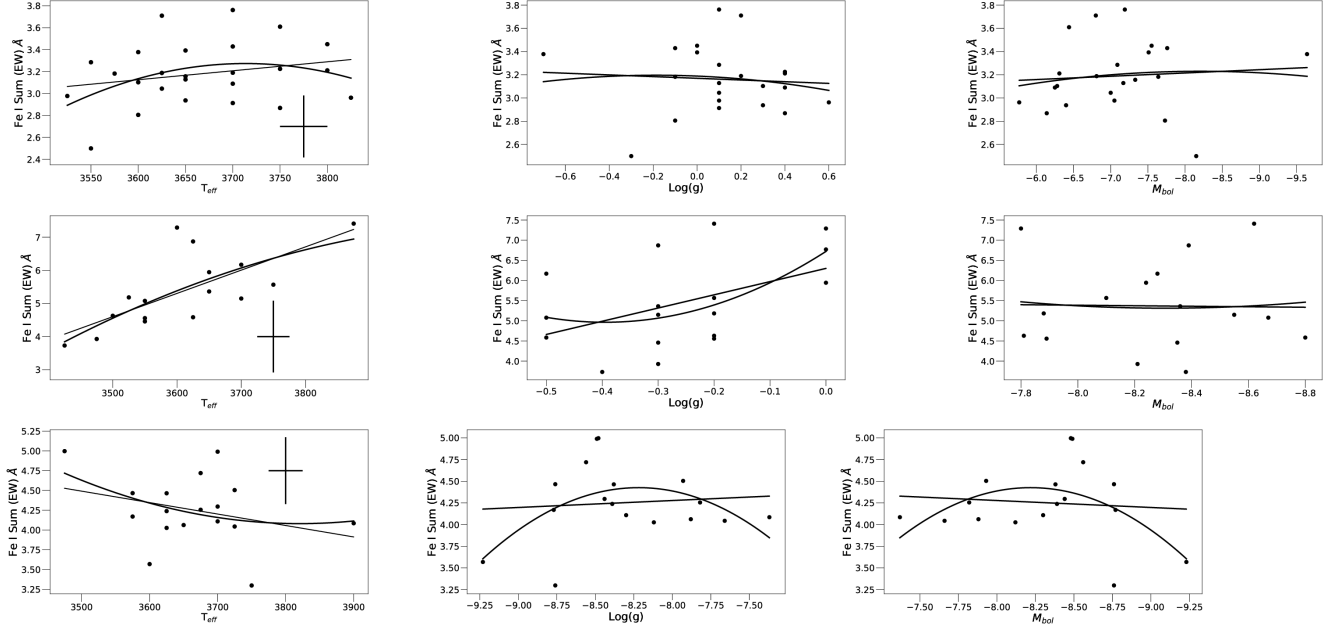


Figure 6. As in Figure 2, but for the sum of the Fe I absorption features.

Hunter, J. D. 2007, *Computing In Science & Engineering*, 9, 90

Jennings, J., & Levesque, E. M. 2016, *ApJ*

Johnson, H. L. 1964, *Bol. Obs. Tonantzintla y Tacubaya*, 3, 305

—. 1966, *ARA&A*, 4, 193

Jones, E., Oliphant, T., Peterson, P., & Others. 2001, *SciPy: Open source scientific tools for Python*, . <http://www.scipy.org/>

Lee, T. A. 1970, *ApJ*, 162, 217

Levesque, E. M. 2018, *ApJ*, 867, 155

Levesque, E. M., Massey, P., Olsen, K. A. G., et al. 2005, *ApJ*, 628, 973

—. 2006, *ApJ*, 645, 1102

Levesque, E. M., Massey, P., Zytkow, A. N., & Nidia, M. 2014, *MNRAS*, 307, 57

Mallik, S. 1996, *A & A*, 124, 359

Massey, P., Nuegent, K. F., & Levesque, E. M. 2017, *Philosophical Transactions of the Royal Society of London Series A*, 375, 20160267

Massey, P., & Olsen, K. 2003, *AJ*, 126, 2867

Patrick, L. R., Evans, C. J., Davies, B., et al. 2017, *MNRAS*, 468, 492

—. 2015, *ApJ*, 803, 14

—. 2016, *MNRAS*, 458, 3968

Pérez, F., & Granger, B. E. 2007, *Computing in Science and Engineering*, 9, 21. <http://ipython.org>

Sakari, C. M., & Wallerstein, G. 2016, *MNRAS*, 456, 831

Smith, G., & Drake, J. J. 1990, *A & A*, 231, 125

Taberner, H. M., Dorda, R., Negueruela, I., & Gonzalez-Fernandez, C. 2018, *MNRAS*, 476, 3106

Tody, D. 1986, *Instrumentation in Astronomy VI*, 733

—. 1993, *Astronomical Data Analysis Software and Systems*, 52

Van Der Walt, S., Colbert, S. C., & Varoquaux, G. 2011, *Computing in Science & Engineering*, 13, 22

Wang, S., Hildebrand, R. H., Hobbs, L. M., et al. 2003, *Instrument Design and Performance for Optical/Infrared Ground-based Telescopes*, 4841, 1145

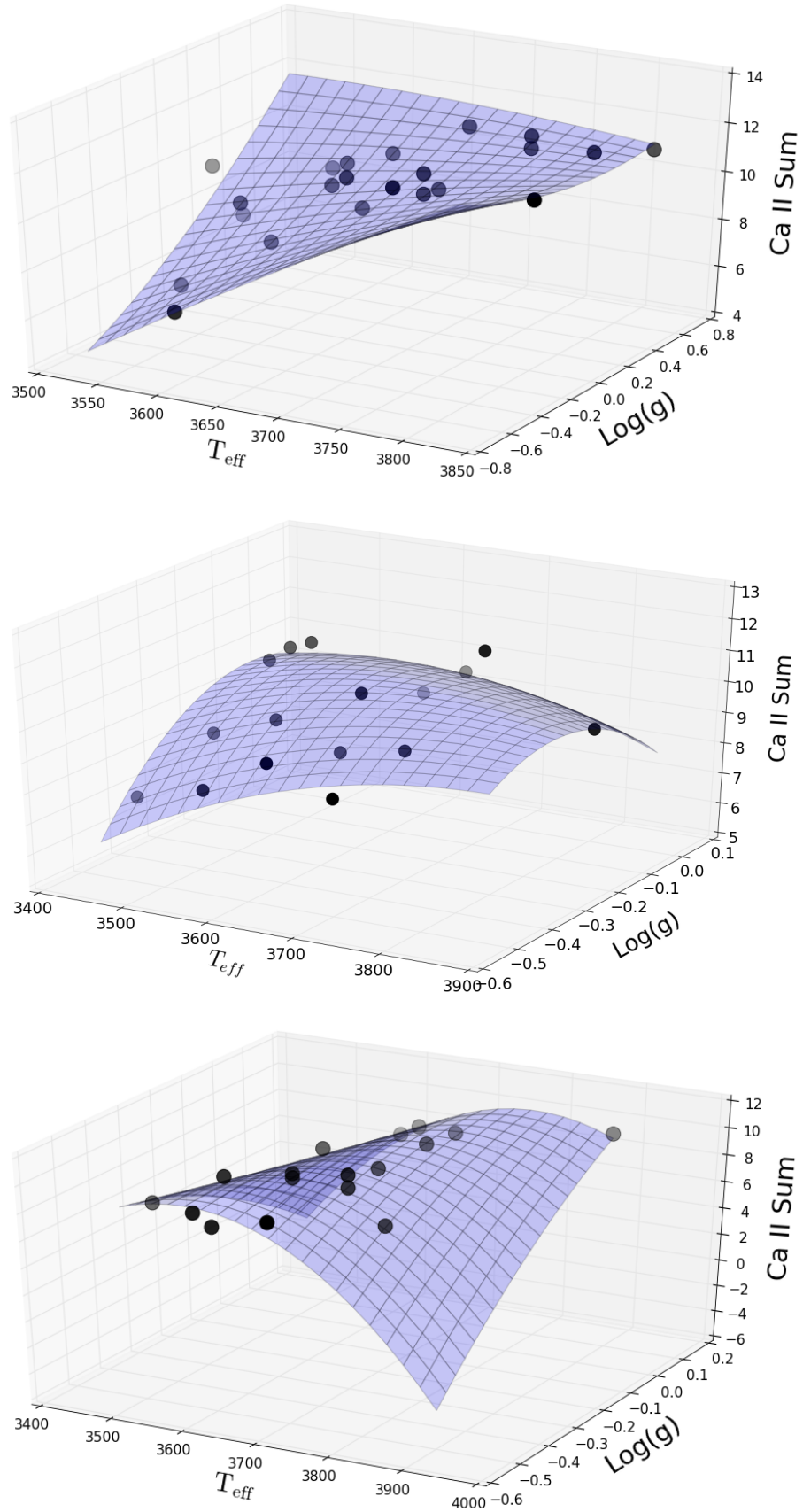


Figure 7. 3D comparison of T_{eff} vs. CaT EW vs. $\log g$ for our MW (top), LMC (center), and SMC (bottom) data, with the best quadratic plane fit illustrated by the blue grid. Darkness of the points indicates “closeness” to the viewer.

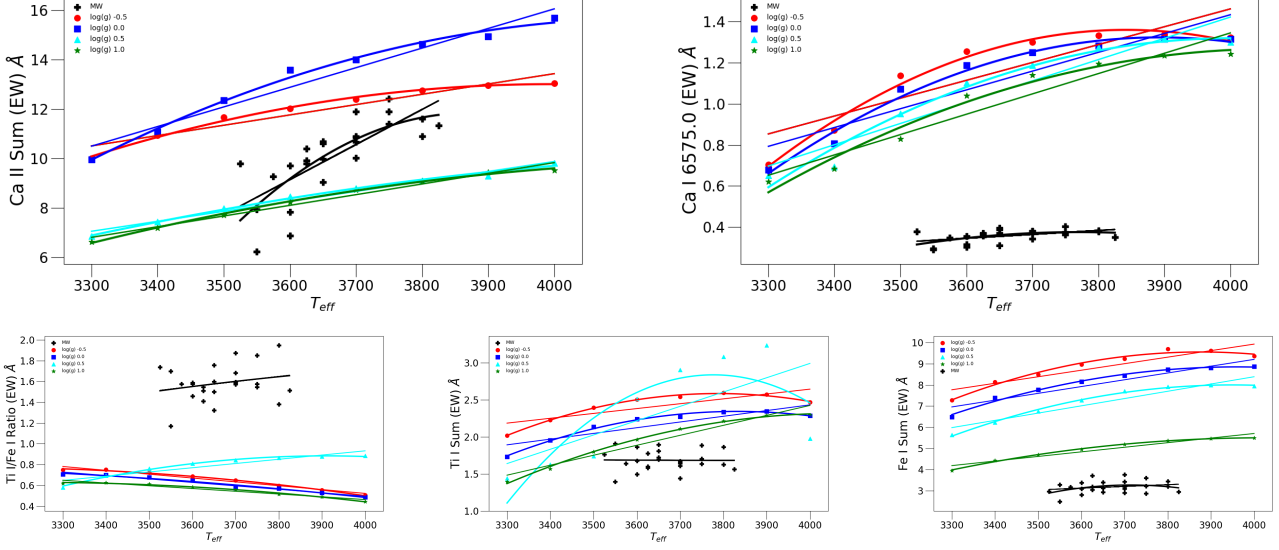


Figure 8. Comparing EW vs. T_{eff} as measured from the Milky Way MARCS stellar atmosphere models for the CaT (top left), Ca I (top right), Ti I/Fe I ratio (bottom left), Ti I sum (bottom center), and Fe I sum (bottom right). Colors indicate the four different values of $\log g$ available in the MARCS models: -0.5 (red), 0.0 (blue), 0.5 (real), and 1.0 (green). Our observed data are also plotted for comparison in black. Best linear and quadratic fits are indicated by solid lines.

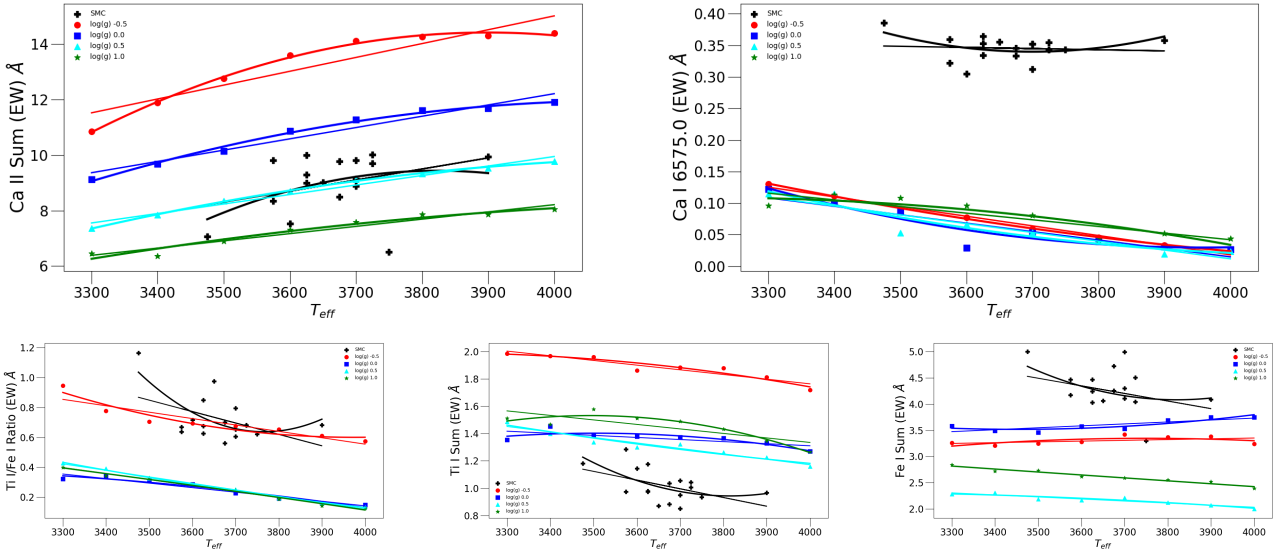


Figure 9. As in Figure 8, but for LMC models and data.

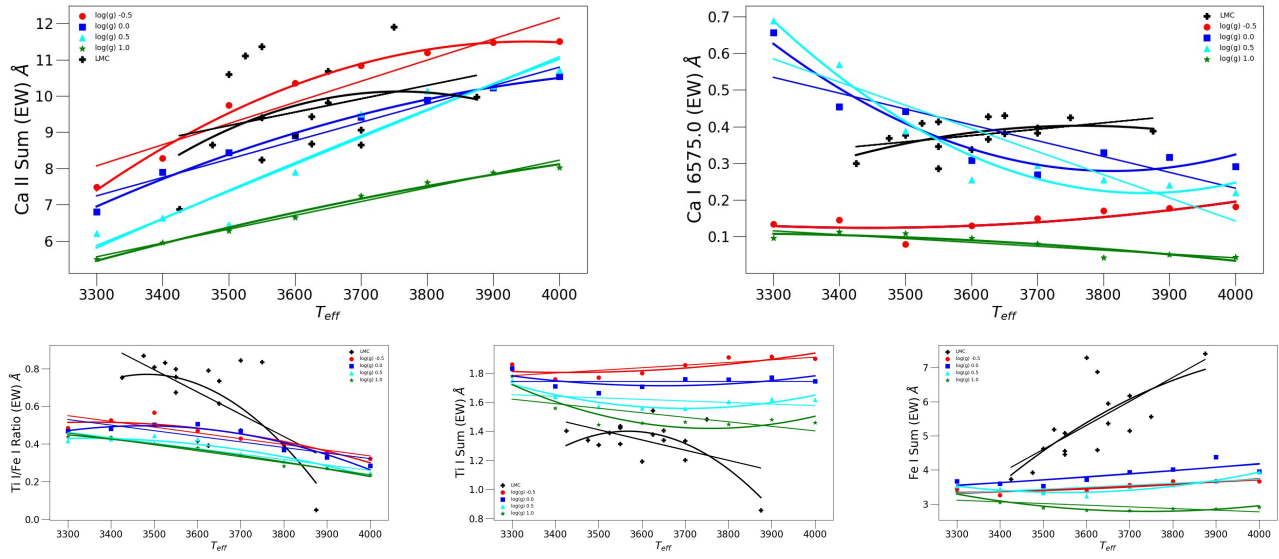


Figure 10. As in Figure 8, but for SMC models and data.